University of Louisville

ThinkIR: The University of Louisville's Institutional Repository

Electronic Theses and Dissertations

12-2008

Redox-regulated ethylene binding to a rhenium-thiolate complex.

Kagna Ouch 1983-
University of Louisville

Follow this and additional works at: https://ir.library.louisville.edu/etd

Recommended Citation

Ouch, Kagna 1983-, "Redox-regulated ethylene binding to a rhenium-thiolate complex." (2008). *Electronic Theses and Dissertations.* Paper 1086.
https://doi.org/10.18297/etd/1086

REDOX-REGULATED ETHYLENE BINDING

TO A RHENIUM-THIOLATE COMPLEX

By

KAGNA OUCH

A Thesis
Submitted to the Faculty of the
Graduate School of the University of Louisville
in Partial Fulfillment of the Requirements
for the Degree of

Master of Science

Department of Chemistry
University of Louisville
Louisville, Kentucky

December, 2008

REDOX-REGULATED ETHYLENE BINDING

TO A RHENIUM-THIOLATE COMPLEX

By

Kagna Ouch
B.A., Royal University of Phnom Penh, 2004

A Thesis Approved on

November 04, 2008

by the following Thesis Committee:

_____
Advisor: Dr. Craig A. Grapperhaus

_____
Dr. Mark E. Noble

_____
Dr. Richard P. Baldwin

_____
Dr. Cindy K. Harnett

DEDICATION

This thesis is dedicated to my parents

Mr. Sokban Ouch

and

Mrs. Kim Lim

who have given me invaluable educational opportunities.

ACKNOWLEDGEMENTS

I would like to thank my advisor Dr. Grapperhaus, for his patience, insight and the opportunity to join his group for this research over the past few years. Being a part of his group has helped me develop as a chemist and analytical thinker. Dr. Gapperhaus also pushed me to reach my potential, even when I doubted myself.

I would also like to thank all my committee members Dr. Noble, Dr. Baldwin and Dr. Harnett for their advice and for their time in evaluating my thesis. Special thanks to Dr. Mark Mashuta for his X-ray expertise and Dr. Neal Stolowich for the help with NMR collection.

I would like to thank the members of the Grapperhaus research group, both past and present: Martin O'Toole, Cesar Masita and Kiran Venna. I am grateful for their support and their friendship.

Finally, I would like to give a big thanks to my parents and sibling who made all of my dreams possible and stood behind my every decision.

ABSTRACT

REDOX-REGULATED ETHYLENE BINDING TO

A RHENIUM-THIOLATE COMPLEX

Kagna Ouch

November 04, 2008

This thesis reports the reactivity of the rhenium-thiolate complex, tris(2-diphenylphosphinobenzenethiolato)rhenium(III), [Re(DPPBT)$_3$] (1) and its oxidized derivatives with ethylene. The reactivity has been studied by electrochemical, spectroelectrochemical, and chemical methods. Based on the cyclic voltammetric data, (1) shows two reversible one electron oxidations and a single reduction. The three redox events are observed at potentials of 420, -340 and -1620 mV versus a ferrocene reference. The events span formal oxidation states from Re(II) to Re(V) although significant ligand participation in the redox events makes these formal assignments misleading with respect to the electronic structure of the complexes. Bulk oxidation of (1) (E$_{applied}$ = +23 mV) in the presence of ethylene yields {[(ethane-1,2-diylbis(thio-2,1-phenylene)diphenyl-phosphino)(2-diphenylphosphinobenzenethiolato)]rhenium(III)} (6) from the addition of the alkene across cis sulfur sites. Electronic spectra recorded during the oxidation reveal two stages. The first stage is assigned as the one electron oxidation of (1) to tris(2-diphenylphosphinobenzenethiolato)rhenium(IV) (3), which is indicated by the intensity increases at 390 and 581 nm. During the second stage, a reaction occurs between (3) and ethylene that yields {[(ethane-1,2-diylbis(thio-2,1-phenylene)diphenyl-phosphino)(2-

diphenylphosphinobenzenethiolato)]rhenium(II)} **(5)**, which is oxidized to **(6)** as shown by the intensity loss at 390 and 581 nm and simultaneous intensity gain at 484 nm. The formal Re(III)/Re(II) reduction potential of **(6)** is shifted approximately +1520 mV consistent with the formation of two thioether donors. Complex **(6)** is stable in solution, but reduction at an applied potential of -977 mV initiates C-S bond cleavage and release of ethylene. The spectroscopic results reveal the pathway to be the reverse of the C-S bond formation. Oxidation of **(1)** using $AgPF_6$ followed by an ethylene purge yields **(6)[PF$_6$]**. The +ESI-MS of **(6)[PF$_6$]** shows a parent ion peak at m/z = 547.0710 (z = 2). The complex **(6)[PF$_6$]** crystallizes as a long thin orange plate in the monoclinic space group *C2/c* with unit cell dimensions of a = 29.009(18) Å; b = 22.577(18) Å; c = 43.99(3) Å; and β = 96.182(17)°. The kinetic and equilibrium parameters associated with C-S bond formation/cleavage were extracted from cyclic voltammograms at multiple scan rates using the DigiSim software package. The rate constants for C-S formation between **(3)** and ethylene, k_f, and for C-S bond cleavage for **(5)**, k_r, were extracted from simulation of the CV data at 7 scan rates ranging from 100 to 1000 mV/s for 3 independent trials. Average values for k_f and k_r are $(1.2 \pm 0.2) \times 10^{-1} \, M^{-1} \, s^{-1}$ and $(3.0 \pm 0.4) \times 10^{-2} \, s^{-1}$, respectively. From these, K_2 was calculated as 4.0 ± 0.8 in agreement with predictions from the UV-visible study. K_1 and K_3 are equilibrium constants for ethylene binding/release between **(1)** and {[(ethane-1,2-diylbis(thio-2,1-phenylene)diphenyl-phosphino)(2-diphenyl-phosphinobenzenethiolato)]rhenium(I)} **(8)**, and tris(2-diphenylphosphinobenzenethiolato)rhenium(V) **(4)** and **(6)**, respectively. From the redox potentials and the equilibrium constant K_2, values for K_1 and K_3 were determined. K_1 has a calculated value of $(1.9 \pm 0.4) \times 10^{-11}$ consistent with observation of an unstable C-S

bond. In contrast, the calculated value of K_3, $(2.5 \pm 0.9) \times 10^9$, is large and is consistent with the observed stability of **(6)**. The large differences in equilibrium constants as a function of oxidation state provide a means to easily gate ethylene addition/release.

TABLE OF CONTENTS

LIST OF FIGURES

LIST OF TABLES

LIST OF SCHEMES

CHAPTER I

INTRODUCTION

Ethylene is the simplest unsaturated hydrocarbon and is classified as an alkene or olefin. Although small in molecular weight, it is the largest organic molecule in terms of industrial production.[1] As shown in Scheme I-1, annual U.S production of ethylene has averaged 24 million metric tons since 1999, and worldwide production in 2007 was estimated as 81 million metric tons.[2,3] The large scale production of ethylene is required since it is a feedstock for polyethylene, ethylene oxide, ethylene chloride and other products. Also ethylene is used for welding, anesthetic agent, and fruit ripening. Ethylene is manufactured by various methods such as thermal cracking of hydrocarbons, catalytic pyrolysis, membrane dehydrogenation of ethane, and other methods.[4]

Mainly, ethylene is produced from thermal cracking of naphtha in the petrochemical industry. Scheme I-2 outlines the basic steps in the process.[5] Naphtha feedstock is heated up to 750-950 °C. This process converts large hydrocarbons to small and unsaturated molecules. Then, this step passes by compression and distillation resulting in cracked gas stream. Cryogenic treatment is used to cool down the cracked gas stream. The gas stream is then separated by two fractionators. The first is the ethylene fractionator, and the second is the propylene fractionator. For this thesis, only the ethylene fractionator is of interest. All of the cold cracked gas stream transfers through the demethanizer tower which produces an overhead consisting of hydrogen and

methane. Methanation is used to purify hydrogen. The pure hydrogen is withdrawn from the lowest temperature stage separator. The bottom stream from the demethanizer tower goes to the deethanizer tower. This tower contains C_2's that are sent to a C_2 splitter. The ethylene product obtained from the overhead of the tower is subjected to acetylene removal and hydrogenation to purify the ethylene. Ethane is also obtained as base product from the C_2 splitter. Overall, this process is energy-intensive and costly.[6] As world energy prices increase and ethylene production remains high, there is increased need to improve efficiency.

U.S. Ethylene Production
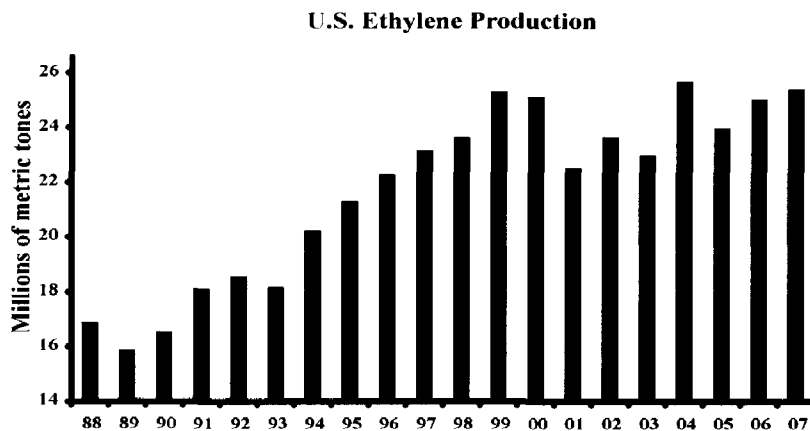
Scheme I-1. U.S. ethylene production recorded from 1988 to 2007. Data obtained from C&E News.[2,3]
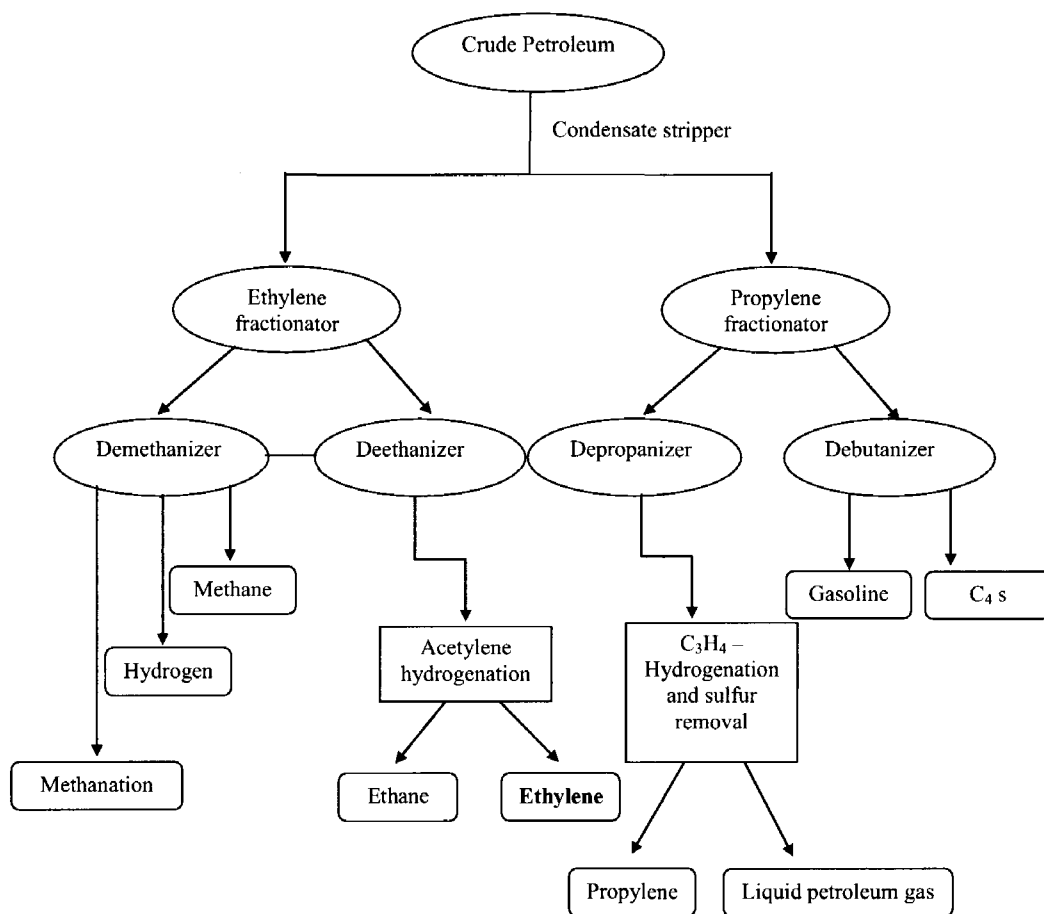
Scheme I-2. Flow diagram for separation of ethylene from other thermal cracking products.

An alternated separation technique involves chemically specific reagents that react with ethylene reversibly. Several schemes using redox-active metal complexes have been studied. The separation of ethylene from poisonous by-products was first studied by Suzuki.[7] Using redox-active salt copper(I) triflate, reacted with vinyl sulfonate anion to increase alkene binding affinity, ethylene and other alkenes were separated from alkanes in the feed. The binding and release of ethylene were observed by a chemical shift in the proton NMR and was followed by purging ethylene and nitrogen through the solution. Moreover, the cyclic voltammograms for both nitrogen and ethylene atmospheres showed a quasi-reversible Cu(II)/Cu(I) couple that the formal potential shifted more positive. The

positive shifts in formal potential are consistent with the proton NMR which indicated a weak, reversible complexation of ethylene with the Cu(I). However, CO and H_2S poisoned the system. This system is interesting as Cu(I) also plays an important role as a cofactor for high-affinity ethylene binding in exogenously expressed ETR1 receptors. ETR1 is one of five ethylene receptor proteins in plants. Ethylene serves a plant hormone affecting seed germination, fruit ripening, and other processes.[8]

Dimeric molybdenum complexes with sulfide ligands were reported by Rakowshi DuBois *et al.* The dimeric complex contains two thiolate bridges and two bridging sulfides. The reactive bridging sulfido ligands are constrained in a cis configuration resulting in coordination of alkenes (Scheme I-3). Similar reactions are observed for hydrogen and alkynes. However, these systems are not tolerant of H_2S and CO.[9]
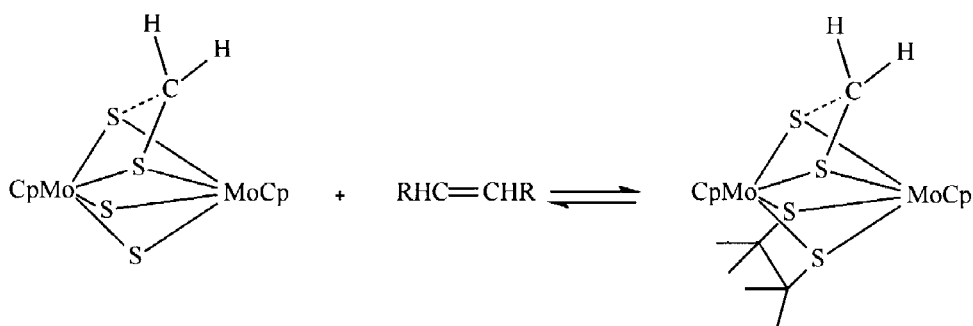
Scheme I-3. Reversible addition of alkenes to $(CpMo)_2(S_2CH_2)S_2$.

Stiefel and coworkers reported binding of ethylene to an oxidized nickel dithiolene with subsequent release upon reduction (Scheme I-4 dark lines).[10] Inter-ligand addition resulted in formation of an S_4^{2-} chelate for nickel which was reportedly stable unless reduced. However, later studies revealed that the reaction is more complex (Scheme I-4 dashed lines). Deleterious intra-ligand ethylene addition, leading to

dihydrodithiin and complex degradation, dominates while the desired inter-ligand addition is a minor product.[11] In studies by Geiger, complications regarding the ethylene release were noted. The potential required for ethylene release was also able to reduce the initial nickel dithiolene leading to decomposition products.[12]
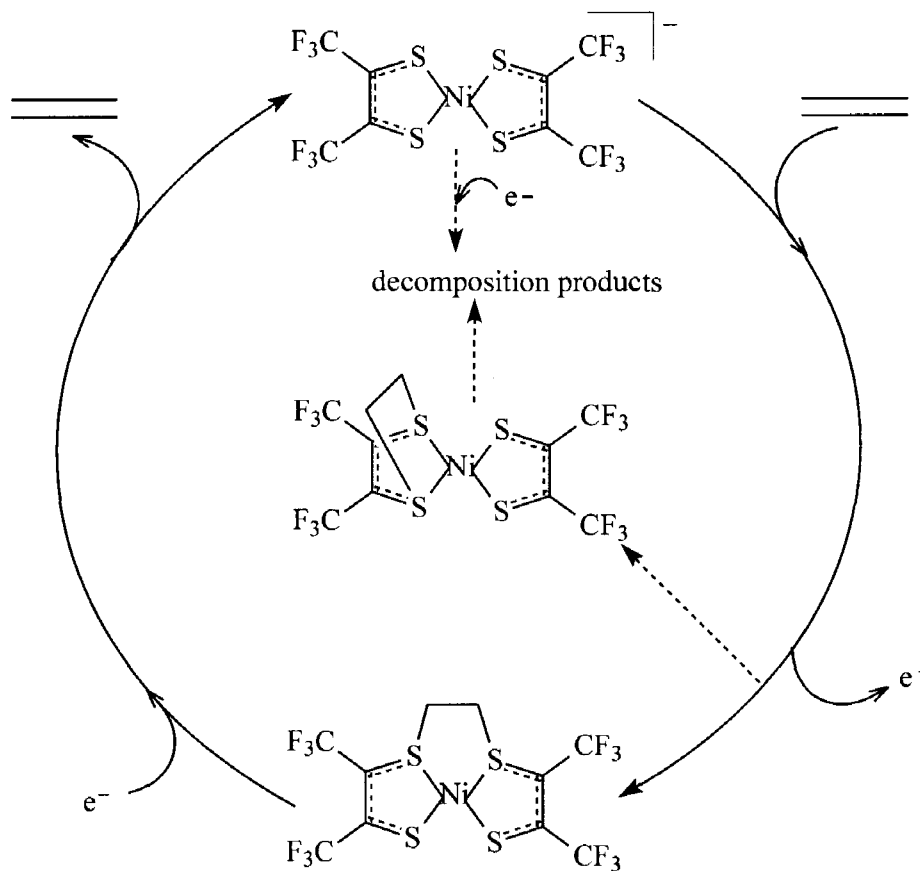
Scheme I-4. Redox initiated ethylene binding/release. The solid lines represent the desired pathway. The dashed lines show competing paths leading to decomposition.

Our approach is to use metal thiolate complexes to overcome the problems displayed by the dithiolene system. Metal thiolates are found in numerous biological systems. The role of the sulfur depends heavily on the identity of the metal and the other ligands that are present (Scheme I-5). For example, zinc finger proteins contain a N_2S_2Zn zinc-dithiolate core which serves structural purposes that is relatively unreactive.[13] MeTe

and Ada proteins contain a $[S_4Zn]^{2-}$ core that is utilized in DNA repair.[14] The thiolate in these cases is nucleophilic and undergoes S-methylation. Moreover, rubredoxins which serve as electron transfer agents contain an $[S_4Fe]^{2-}$ core with a tetrahedral iron coordinated by four cysteines.[15]

Scys
|
cysS —Zn
/ \Nhis
Nhis

Zinc Finger protein
from GATA family

Scys
|
cysS —Zn
/ \Scys
cysS

Ada DNA repair
protein

Scys
|
cysS —Fe
/ \Scys
cysS

Rubredoxin
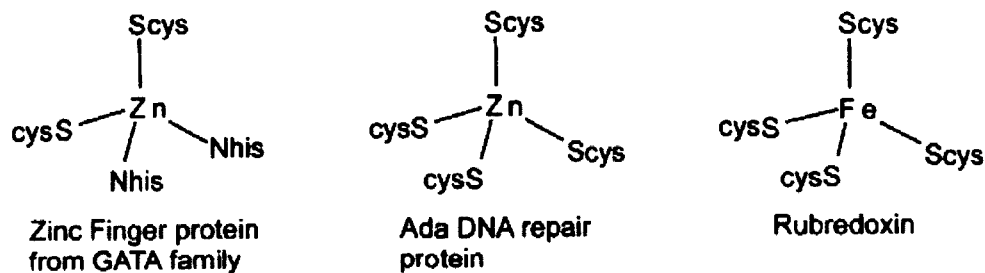
Scheme I-5. The functional site of zinc and iron proteins with a pseudo-tetrahedral cysteine-rich environment.

The reactivity of the thiolate has been attributed to the interaction of the sulfur p lone-pair with a "t_{2g}" metal d-orbital.[16,17] As shown in Scheme I-6, there are three general cases for these interactions depending on the relative energies of the orbitals. When the metal d-orbital and sulfur p lone-pair have similar energies, (Scheme I-6a), there is a strong interaction that yields a significantly stabilized π-bonding orbital and a significantly stabilized π-anti-bonding orbital. Each of these orbitals has significant sulfur and metal character. Although there is no net π-bond, the increased energy of the anti-bonding orbital "activates" the thiolate nucleophilicity. Further, since the orbital is not localized on the metal or sulfur, it is difficult to assign oxidations as metal- or ligand-centered when an electron is removed. Rather, "metal stabilized thiyl radicals", or complexes that enjoy increased stability but maintain some reactive properties of thiyl radicals are generated.

6

When the sulfur p lone-pair orbital has higher energy than the t_{2g} metal d-orbital there is no significant interaction between the two. The higher energy orbital is sulfur-centered and may be nucleophilic, but it is not "activated" (Scheme I-6b).[16] Oxidation would be expected to be sulfur based. When the t_{2g} metal d-orbital is higher in energy than the sulfur p-orbital, there is also no significant interaction. The thiolate is not expected to be as nucleophilic, and oxidation is regarded as metal-based (Scheme I-6c).
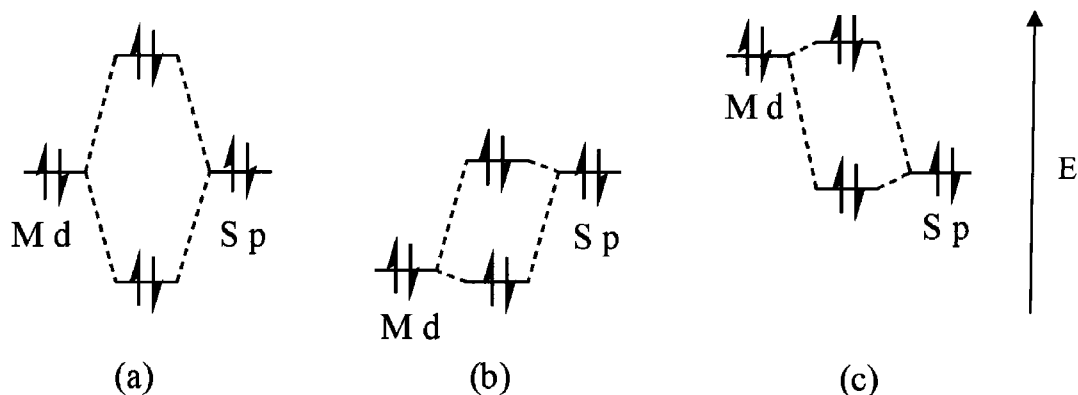
Scheme I-6. Partial molecular diagrams are showing interactions of metal d-orbital and sulfur p orbital to generate a π-bonding and π-anti-bonding orbitals.

Reactions of organic thiyl radicals typically correspond to one of three major classes (Scheme I-7). First, thiyl radicals may react with each other forming a disulfide. Second, thiyl radicals can abstract hydrogen from activated C-H bonds. Finally, thiyl radicals can react with unsaturated hydrocarbons in a C-S bond forming reaction.[18] Carbon–sulfur bond formation between organic thiyl radicals and unsaturated hydrocarbons has been exploited for cis/trans isomerization, sulfide synthesis, and polymerization. In 1958, Helmreich and coworkers reported thiyl radical initiated isomerization of cis-alkenes to trans-alkenes in a reversible reaction.[19] The addition of

thiyl radicals to alkenes to form C-S bond was utilized by the Ichninose group for the synthesis of sulfides.[20] Apart from the C-S bond formation reaction, thiyl radicals have also been used in the initiation of block polymerization.

$$RS \cdot \begin{cases} \xrightarrow{RS^\bullet} RS\text{-}SR \\ \xrightarrow{R'\text{-}H} RS\text{-}H + R \cdot \\ \xrightarrow[R'_2C=CR'_2]{} RSCR'_2\dot{C}R'_2 \end{cases}$$
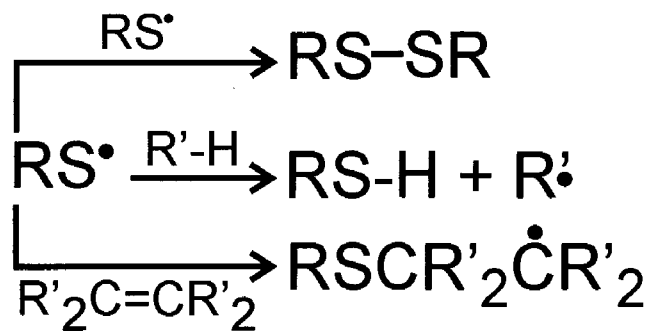
Scheme I-7. Three major reactions for organic thiyl radicals.

The object of this thesis is to use metal-thiolate to promote C-S bond formation by hindering disulfide formation and H-atom abstraction. Geometric or steric constraints are sufficient to hinder disulfide formation. Hydrogen abstraction from C-H bonds by thiyl radicals is only favored for activated hydrogen atoms since the S-H bond enthalpy typically is weaker than the C-H bond enthalpy.[21] Coordination of the thiolate to a metal should further decrease S-H bond enthalpy.

Previously in the Grapperhaus group, the trithiolate complex $[Ru(DPPBT)_3]^-$ was shown to be a good nucleophile, reacting even with CH_2Cl_2 to generate a dithioether (Scheme I-8).[22] By combined spectroscopic and electrochemical investigations along with computational studies, it was also shown that oxidation yields an intermediate best described as a metal-coordinated thiyl radical, as shown in Scheme I-9.[23-26] In acetonitrile and most other solvents, the radical slowly decays to a proposed disulfide complex.[27] The slow rate is attributed to the orthogonally positioned thiolate p orbitals. Poturovic showed that the intermediate reacts with methyl ketones to generate new C-S bonds.[28] Her work

implicated the enol tautomer of the ketone as the reactive species. These suggested alkenes should also react with the intermediate. This was confirmed by Venna who showed that a variety of alkenes add across the cis sulfur sites to generate dithioether complexes. However, these complexes could not be reduced, and the C-S bonds could not be cleaved.[29]
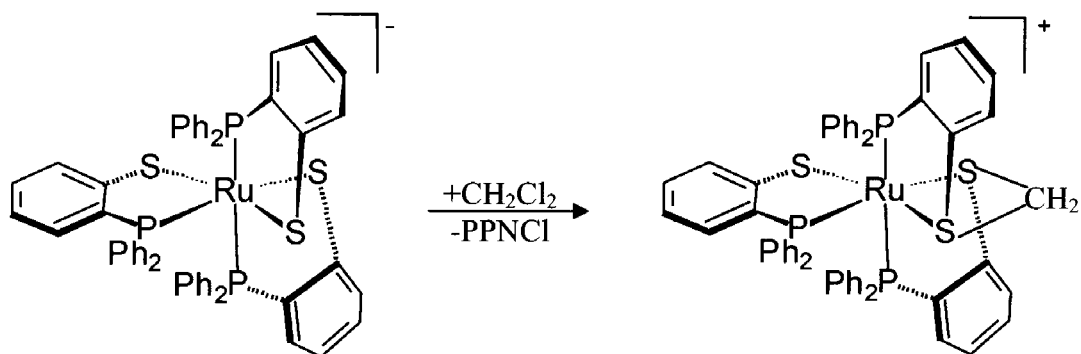
Scheme I-8. The reaction of [Ru(DPPBT)$_3$]$^-$ with dichloromethane.
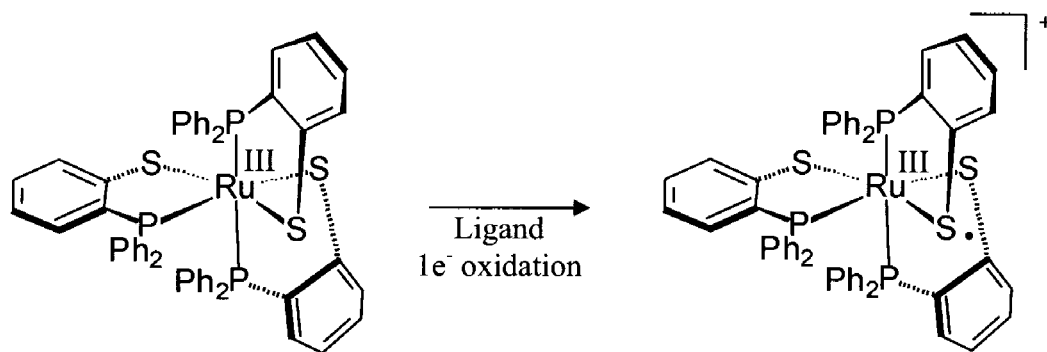
Scheme I-9. Oxidation of [Ru(DPPBT)$_3$] to the reactive intermediate.

The focus of this thesis will be directed towards understanding oxidation and reduction induced C-S formation and cleavage, employing the related rhenium complex [Re(DPPBT)$_3$] **(1)** (DPPBT = 2-diphenylphosphinobenzenethiolate) (Scheme I-10). [Re(DPPBT)$_3$] and [Ru(DPPBT)$_3$]$^+$, the reactive Ru intermediate, are isoelectronic.

Complex **(1)**, previously reported by Dilworth *at el.*, shows two oxidations and one reduction making it is a suitable candidate for investigation of a redox-regulated reversible alkene binding system.[30]
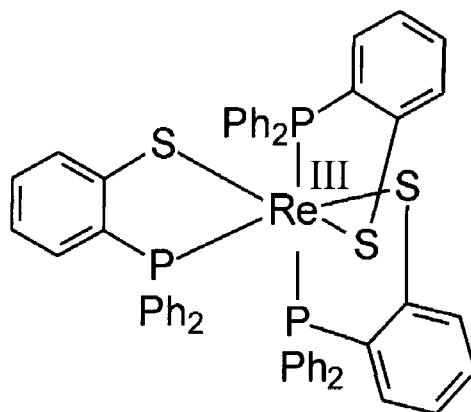
Scheme I-10. Stick representation of [Re(DPPBT)₃] **(1)**. (DPPBT = 2-diphenylphosphinobenzenethiolato).

CHAPTER II

EXPERIMENTAL METHODS

Materials and Physical Methods

All chemicals were purchased from commercial sources (Aldrich, VWR chemicals, TCI, Acros Organic, Alfa Aesar, Strem Chemicals) and used without purification unless otherwise stated. $AgPF_6$ was obtained from Aldrich and stored in an argon filled dry box. The ligand H(DPPBT) was synthesized as the modification as described below.[31] The complex as $[ReOCl_3(PPh_3)_2]$ and $[Re(DPPBT)_3]$ were prepared as described in the literature.[30,32] Ethylene gas (polymer purity 99.9 %) was obtained from Matheson Tri-Gas. All solvents were purified utilizing the standard methods and were freshly distilled immediately before use.[33] Deuterated chloroform was obtained from Cambridge Isotope Laboratories, Inc. and used as received. All reactions were performed under anaerobic conditions via standard Schlenk line techniques unless otherwise noted.

IR spectra were measured with a Thermo Nicolet Avatar 360 spectrometer with a resolution of 4 cm^{-1}. An Agilent 8453 diode array spectrometer was used for all electronic absorption measurements utilizing a custom designed cell with a 0.5 cm path length. Element analysis was performed by the Midwest Microlab (Indianapolis, IN). Mass spectra were collected by the Mass Spectrometry Application and Collaboration Facility in the Chemistry Department at Texas A&M University. X-ray crystallography was conducted by Dr. Mark Mashuta at the University of Louisville's X-ray diffraction

laboratory. X-ray crystallographic data were collected on a Brucker SMART APEX CCD diffractometer. CCDC-699464 contains the supplementary crystallographic data for this thesis. Data can be obtained free of charge from The Cambridge Crystallographic Data Center via www.ccdc.cam.ac.uk/data_request.cif.

Electrochemical Methods

All electrochemical measurements were performed by using a PAR 273 potentiostat/galvanostat with a three-electrode cell (glassy carbon or platinum mesh working electrode, platinum wire/mesh counter electrode, and Ag/Ag^+ pseudo reference electrode). All reported potentials are relative to ferrocenium/ferrocene which was observed at +577 mV versus the pseudo reference.

Cyclic Voltammetry

For cyclic voltammetry experiments, a Dr. Bob's cell was used as a three electrode cell. The Dr. Bob's cell kit was purchased from Gamry Instruments. The cell contains a platinum wire counter electrode, a 6.5 mm diameter glassy carbon working electrode, and an Ag/Ag^+ pseudo reference electrode. The Dr. Bob's cell can be used with solvent volumes from 2 mL to 50 mL and, in typical experiments; a volume of 10 mL was used.

Prior to addition of analyte, background voltammograms were collected using 10 mL of dichloromethane with 0.1 M tetrabutylammonium hexafluorophosphate (TBAHFP) as supporting electrolyte as described below. Nitrogen gas was bubbled through the solution for 5 minutes to remove dissolved oxygen, and then the solution was settled for 2 minutes without disturbing under a nitrogen atmosphere. The initial, switching and final potentials were set between the solvent limits of -1.5 V to 2.0 V

versus the pseudo-reference. Background voltammograms were collected at scan rates of 100, 150, 200, 300, 400, 600, 800, and 1000 mV/s. The window was scanned from negative to positive.

Cyclic voltammograms of the analyte were obtained at a concentration of 1.0 mM. Data was collected at multiple scan rates of 100, 150, 200, 300, 400, 600, 800, and 1000 mV/s with various potential windows. Prior to each scan, the solution was purged with nitrogen for several minutes and then held under a nitrogen atmosphere during analysis. For experiments with ethylene, a similar protocol was used with ethylene replacing nitrogen as the purge and head gas. Three independent samples were analyzed.

Prior to data interpretation, the appropriate background voltammogram was subtracted from the measured sample data. For each set of data, the CV results over all scan rates were fit simultaneously with DigiSim software package.[34] The DigiSim software package was purchased from Bioanalytical Systems. All data were input in a text data file format. Existing data files were converted to the **.use** format as described in DigiSim instruction manual.[35]

The results of data analyses under nitrogen and ethylene in the small window and larger window are described in chapter III. The methods of analysis are described below. The data collected under nitrogen in the "small window" was fit as a single, one electron redox event. Uncompensated resistance was estimated using the method of Bond *et al.*[36] The diffusion coefficient was treated as a variable parameter with an initial setting of 10^{-6} cm^2/s. The standard rate constant (k_s) was treated as a variable parameter with an initial guess estimated by equations 1 and 2. The standard half potential was estimated based on

the potentials of minimum and maximum current and allowed to refine freely. The

transfer coefficient, α, was set to 0.7.[37,38]

$$k_s = \psi * a \quad (1)$$

$$a = (\pi D_0 fv)^{1/2} \quad (2)$$

The data collected under ethylene in the "small window" was fit according to an

ECEE mechanism with three redox events and a single chemical step associated with the

equilibrium constant K defined by k_f and k_r. All available parameters from the simulation

under nitrogen were used as initial settings. The diffusion coefficients of all species were

treated as single, variable parameter. The concentration of ethylene was set to the

literature value (0.4642 M) for saturated dichloromethane solutions.[39] The parameters K

and k_f were estimated from UV-visible studies and allowed to freely refine. The rate

constant, k_r, was calculated from K_2 and k_f.

All fitting parameters were refined simultaneously over all scan rates and reported

values are of the average of three independently prepared samples. Simulation of data

collected in the "big window" under nitrogen and ethylene were similarly treated. This

data is complicated by competing decomposition reactions as described in chapter III.

Bulk Electrolysis

A custom built cell was used for bulk electrolysis and/or spectroelectrochemistry.

The custom cell that was designed by E.Bothe of the Max-Planck Institute für

Bioanorganische Chemie, Mulheim, Germany. The custom cell has a volume of ~ 10 mL

and two quartz windows with a 0.5 cm path length. The sample holder and cell were

situated in custom-built Plexiglas box fitted with Dynasil 4000 quartz windows (Pacific

Quartz) that was purged with nitrogen during low temperature experiments to prevent the

condensation of water on the sample holder. A VMR 1190A chiller was used to lower the temperature for the cell which was adjusted to -35°C and the inside cell temperature was shown to be -15°C. Nitrogen or ethylene gas was bubbled through the solution in order to avoid oxygen diffusion and also to mix the solution. A background square wave voltammogram was determined in dry dichloromethane with supporting electrolyte prior to analyte addition. Bulk electrolysis measurements were performed with platinum mesh working electrode and counter electrodes and an Ag/Ag$^+$ pseudo reference electrode. To record square wave measurements, the platinum mesh working electrode was replaced with a glassy carbon working electrode.

The coulometric data was plotted as current versus time and/or charge versus time. From these plots, a background current and charge could be determined. The experimental charge was calculated by subtracting the background charge from the measured charge. The number of transferred electron equivalents was determined by comparing this value with the theoretical value calculated from Faraday's law. The electronic spectra were collected by carefully positioning the purge tube out of the quartz window at approximately one tenth of total expected charge intervals.

Square Wave Voltammetry

The square wave measurements were performed as described for the bulk electrolysis experiment. After each performed oxidation (or reduction), the working electrode was switched to a glassy carbon electrode and counter electrode was changed to a platinum wire electrode, bubbling was stopped, and a square wave voltammogram was obtained. In all cases, the initial potential was held for 15 seconds prior to initiation of the scan. Data was collected by two ways. The cathodic scan was obtained by input an initial

and final potential from -1.5 V to 2.0 V and anodic scan was vice versa. The resulting peaks were plotted as current versus potential.

Electrochemical Synthesis

[tris(2-diphenylphosphinobenzenethiolato)rhenium(II)] **(2):** The spectroelectro-chemical cell was filled with 10 mL of dichloromethane and 0.387g (0.1 M) of TBAHFP was added to record the backgrounds for both UV-visible spectroscopy and cyclic voltammetry. Then 3.0 mg (3.0 μmol) of [Re(DPPBT)$_3$] **(1)** was added resulting in a burgundy colored solution. Nitrogen was bubbled through the solution to ensure proper mixing followed by applying a potential of -1877 mV. During the reduction, the pink solution was formed as a result of the compound **(2)** product. This compound **(2)** is easily oxidized to **(1)** and reliable coulometric results could not be obtained. No efforts were made to isolate **(2)**. The observed square wave voltammograms were not changed as compared to the original events. The events were shown at 427, -357, and 1600 mV.

[tris(2-diphenylphosphinobenzenethiolato)rhenium(IV)] **(3):** All measurements were performed as described in the synthesis of compound **(2)**. Next, to the solution was applied a potential of +23 mV until the current achieved the baseline. In this first oxidation, -160 mC (0.86 electron equivalent) of charge was produced. As a result, compound **(1)** was converted to a blue compound referred to as compound **(3)** (λ_{max} (nm) = 390, 581). The square wave voltammogram events were observed at 427, -357, and -1600 mV.

[tris(2-diphenylphosphinobenzenethiolato)rhenium(V)] **(4):** The blue solution of compound **(3)** was held under nitrogen atmosphere, then the holding potential for second oxidation was applied at a potential of +723 mV. During the oxidation, the color of the

solution changed to brown forming compound (4) (λ_{max} (nm) = 477). The current decayed until less than 1-5% and the resulting charge was -371 mC (2 electron equivalents). The square wave events were determined at 427, -357, and -1600 mV.

{[ethane-1,2-diylbis((thio-2,1-phenylene)diphenyl-phosphine)](2-diphenyl-phosphinobenzenethiolato)rhenium(II)} (5): Ethylene was purged through a fresh solution of compound (3) for 10 minutes in the fume hood. The square wave voltammogram was recorded at potential of -1099 mV. The solution was developed to purple as the formation of compound (5) and electron absorption was measured at (λ_{max} (nm) = 323). The square wave voltammograms were displayed under ethylene atmosphere and the events were shown at -131, -365, and -1587 mV.

{[ethane-1,2-diylbis((thio-2,1-phenylene)diphenyl-phosphine)](2-diphenyl-phosphinobenzenethiolato)rhenium(III)} (6): Compound (1) was oxidized by an applied potential at +23 mV for one electron while ethylene was purged through the solution. The current was decayed until the oxidation was completed. The resulting orange complex (6) occurred at a potential of -151 mV. The electronic spectra were indicated by the intensity increase at 484 nm. The square wave events were revealed at -131, -365, and -1587 mV.

Chemical Synthesis

{[ethane-1,2-diylbis((thio-2,1-phenylene)diphenyl-phosphine)](2-diphenyl-phosphinobenzenethiolato)rhenium(III)} hexafluorophosphate (7): To a burgundy solution of (1) (30 mg, 28 μmol) in C_6H_5Cl (5 mL) was added $AgPF_6$ (14 mg, 56 μmol). The resulting solution was bubbled with ethylene during which an orange color developed. The mixture was then filtered through wool cotton to remove Ag (s). Within

17

10 minutes (7) precipitates as a fine orange microcrystalline product. The C_6H_5Cl was removed via cannula and the product dissolved in a mixture of CH_2Cl_2 (1.0 mL) and C_6H_5Cl (0.6 mL) under an ethylene atmosphere. Slow evaporation of the solvent yields X-ray quality needles. Yield: 12 mg (40%). Element analysis (%) calcd. for $C_{56}H_{46}P_5F_{12}S_3Re$: C 48.59, H 3.35, obs: C 48.12, H 3.39; +ESI-MS for $C_{56}H_{46}P_5F_{12}S_3Re$: theoretical m/z (Z = 2), 547.0766; observed, 547.0710.

(2-diphenylphosphinobenzenethiol) (DPPBTH): Benzenethiol (6.6 mL, 7 g, 0.064mol) was added dropwise slowly to n-butyllithium solvent (57 mL, 0.142 mol) and N, N, N', N'-tetramethylethylenediamine (22 mL, 0.14 mol) in 100 mL (0.142 mol) of cyclohexane at room temperature under nitrogen atmosphere. The reaction mixture was heated to 70°C for 4 hours under reflux. Filtered precipitate was washed with hexane (100 mL). Tetrahydrofuran (100 mL) in acetone-dry-ice bath at -78°C dissolved precipitate (lithium 2-lithiobenzenethiolate). Treatment of precipitate in ice bath with chlorodiphenylphosphine (8.41 mL, 0.045mol) was dropped around 2 hours. The mixture was stirred for 24 hours at room temperature. The reaction mixture was diphenylphosphine 2-lithiobenzenethiolate which was quenched with aqueous hydrochloric acid (30 mL HCl and 170 mL distilled water) to protonate and dry in vacuo. The resulting product was added by distilled water (150 mL) and 300 mL diethyl ether. The water layer was extracted with ether. The ether layer was then dried with $MgSO_4$ and the ether was removed to give the indicated products (2-diphenylphosphinobenzenethiol). Yield: 1.308g. ^{1}H NMR (CD_2Cl_2): σ (ppm) = 7.3-6.7 (14H, m), 4.00 (1H, SH). ^{31}P NMR (CD_2Cl_2) σ (ppm) = -11.73.

[oxotrichlorobis(triphenylphosphine)rhenium(V)] **[ReOCl₃(PPh₃)₂]:** Triphenyl-phosphine (5 g) in 10 mL ethanol was boiled around 2 hours. A boiling solution of perrhenic acid (1 g) and concentrated hydrochloric acid (1 mL) was added to triphenylphosphine solution. Then the mixture was heated and stirred for 3-5 minutes. A greenish-yellow precipitate formed. Then the product was filtered with the gravity filtration method. The indicated product was yellow crystal of [ReOCl₃ (PPh₃)₂] and the green impurity was removed by recrystallization. The product was dried, giving [ReOCl₃ (PPh₃)₂] yield 85 % (0.861 g, 0.001 mol). IR (KBr pellet), cm^{-1}: 1479 (m), 1434 (m), 1193 (s), 1095 (m), 972 (m), 751 (m), 694 (m), 523 (m).

[tris(2-diphenylphosphinobenzenethiolato)rhenium(III)] **[Re(DPPBT)₃] (1):** 0.11 g (0.036 mmol) DPPBTH (2-diphenylphosphinobenzenethiol) in 0.7 mL triethylamine was added to 0.1 g (0.12 mmol) [ReOCl₃ (PPh₃)₂] in methanol (25 mL). The mixture was heated and stirred under reflux for 30 minutes. The precipitate was filtered under gravity. The burgundy product was washed with ethanol and diethyl ether and dried in vacuo. Yield: 75 % (0.096 g, 0.09 mmol). The square wave voltammetry showed events at 427 mV, -357 mV and -1600 mV.

CHAPTER III

RESULTS AND DISCUSSION

As described in Chapter I, the Ru-thiolate complex [Ru(DPPBT)$_3$] adds ethylene and related alkenes upon oxidation to yield stable Ru(II)-dithioether complexes. The C-S bond forming reaction is stoichiometric with good yields. However, the complex cannot be reduced, and no route for C-S bond cleavage could be identified. In an unrelated study by Rothlisberger, C-S bond cleavage for rhenium, technetium, and ruthenium dithioether complexes was investigated using computational methods. For the hexathioether complexes of [M(9S3)$_2$]$^{2+}$ (M = Re, Tc, and Ru; 9S3 = 1, 4, 7 trithiacyclononane), the detailed structural and electronic characterization of these complexes and their reductive C-S bond cleavage reactions was determined by Density Functional Theory (DFT) calculations and first-principles molecular dynamics studies. Overall, C-S cleavage is initiated by metal-centered reduction as shown in Scheme III-1. For Ru(II) complexes, C-S cleavage is impractical due to the stability of t$_{2g}^6$ electron configuration. For Re(II) and Tc(II), reduction to M(I) results in a stable t$_{2g}^6$ electron configuration and occurs more readily.[40,41]

20
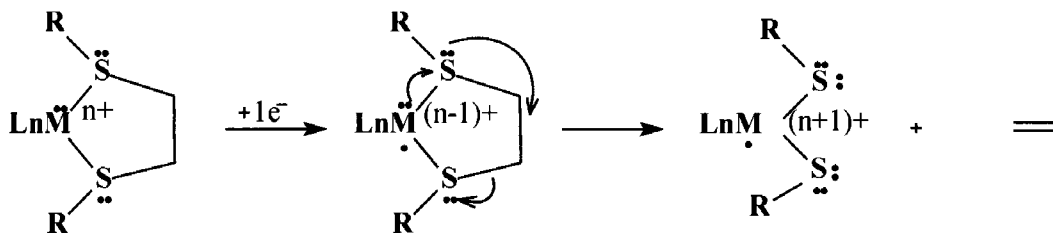
**Scheme III-1.** Metal centered reduction induces C-S bond cleavage/alkene

The rhenium derivatives of $[Ru(DPPBT)_3]^{n+}$ were previously reported by Dilworth *et al.* from a variety of rhenium sources.[30] Tris(2-diphenylphosphino-benzenethiolato)rhenium(III), $[Re(DPPBT)_3]$ **(1)** can be isolated as dark burgundy monoclinic crystals. The UV-vis spectrum displays bands at $\lambda_{max} = 323$ and 534 nm in dichloromethane, and the mass spectrum shows the expected parent peak at m/z = 1066. The cyclic voltammogram of **(1)** was reported to display two reversible one electron oxidations and a reversible one electron reduction. The three reversible redox couples were recorded at potentials of -990, +230, and +1010 mV versus an Ag pseudo-reference. Each was assigned by Dilworth as a metal-based event spanning oxidation from Re(II) to Re(V), although the possibility of ligand-centered redox activity was noted.

The work described hereafter was undertaken to investigate reversible C-S bond formation/cleavage between ethylene and [Re (DPPBT) 3] **(1)** and its oxidized derivatives as a function of oxidation state (Scheme III-2). All relevant thermodynamic parameters, expressed as redox potentials or equilibrium constants, are detailed in Chapter II summarized in Table III-1.

21
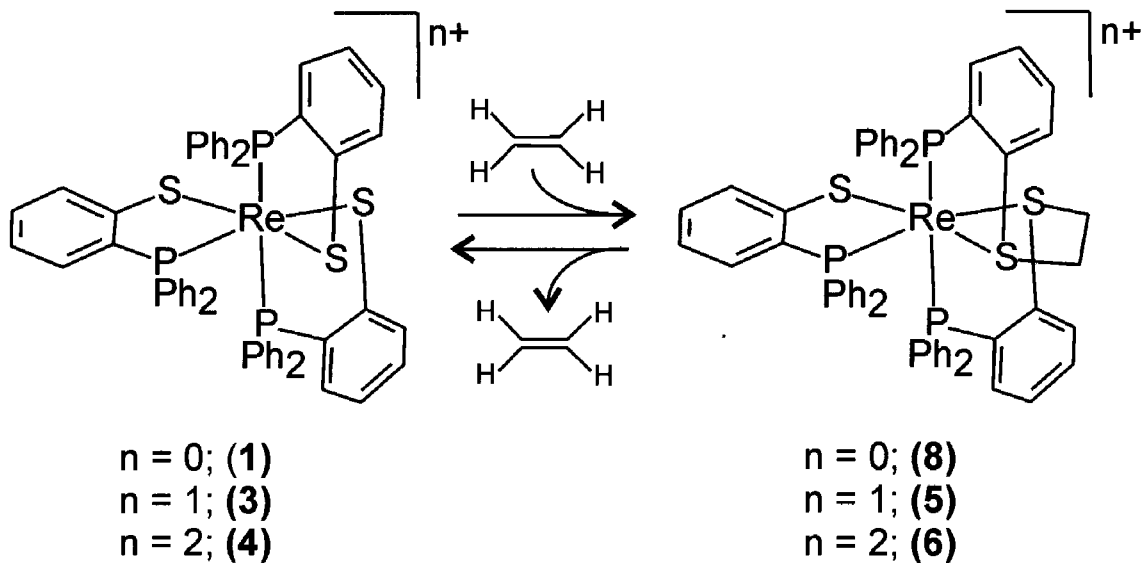
Scheme III-2. Reversible C-S bond formation/cleavage between **(1)**, **(8)**, and oxidized derivatives.
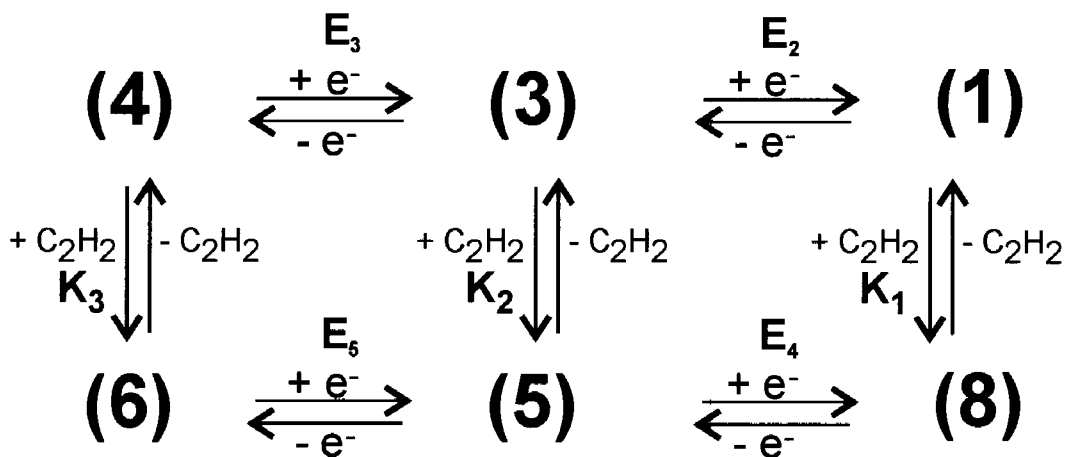
Scheme III-3. Square representation of C-S bond formation/cleavage and electron transfer.

Table III-1. Summary of standard reduction potentials and formal oxidation state assignments for **(1)**, **(8)**, and their derivatives.

	Half reaction	Formal Re Ox. State	$E_{1/2}$ (mV)	ΔE (mV)
E_1	**(1)/(2)**	Re (III)/Re (II)	-1610	140
E_2	**(3)/(1)**	Re (IV)/Re (III)	-340	117
E_3	**(4)/(3)**	Re (V)/Re (IV)	420	143
E_4	**(5)/(8)**	Re (II)/Re (I)	-1010	irreversible
E_5	**(6)/(5)**	Re (III)/Re (II)	-100	91

Using the methods reported by Dilworth, **(1)** was synthesized and purified for electrochemical analysis. A 1 mM solution of **(1)** in CH_2Cl_2 (10mL) was prepared with 0.1 M TBAHFP as supporting electrolyte. Figure III-1 shows the recorded cyclic voltammogram at a scan rate of 200 mV/s under a nitrogen atmosphere. The potentials were recorded versus a Ag pseudo-reference and scaled to a ferrocenium/ferrocene standard by using an internal standard. Overall, our results reproduce those previously reported, although the values from the two studies are reported versus different references. Versus a ferrocene reference, the oxidation events of **(1)** were observed at -340 mV (E_2) for the **(3)/(1)** couple, 420 mV (E_3) for the **(4)/(3)** couple. A single reversible one electron reduction to **(2)** was also shown at -1610 mV (E_1).

Figure III-1. Cyclic voltammogram of 1mM complex **(1)** obtained under a nitrogen atmosphere in dichloromethane at room temperature with 0.1 M TBAHFP as supporting electrolyte. The initial and final potentials were set to -2000mV with a switching potential of 1000mV. The initial potential was applied for 15 seconds before the scan. Potential referred to a ferrocenium/ferrocene reference (E_{obs} = +577mV).* is indicated as the impurity.

For a fresh 1 mM solution of **(1)** the cyclic voltammogram was recorded under an ethylene atmosphere. Ethylene was bubbled through the solution for 1 or 2 minutes, and the solution was allowed to stand under an ethylene atmosphere. The voltammogram was collected over a wide potential that was scanned from negative to positive potentials. As shown in Figure III-2, the CV shows two new peaks in addition to those observed under ethylene.
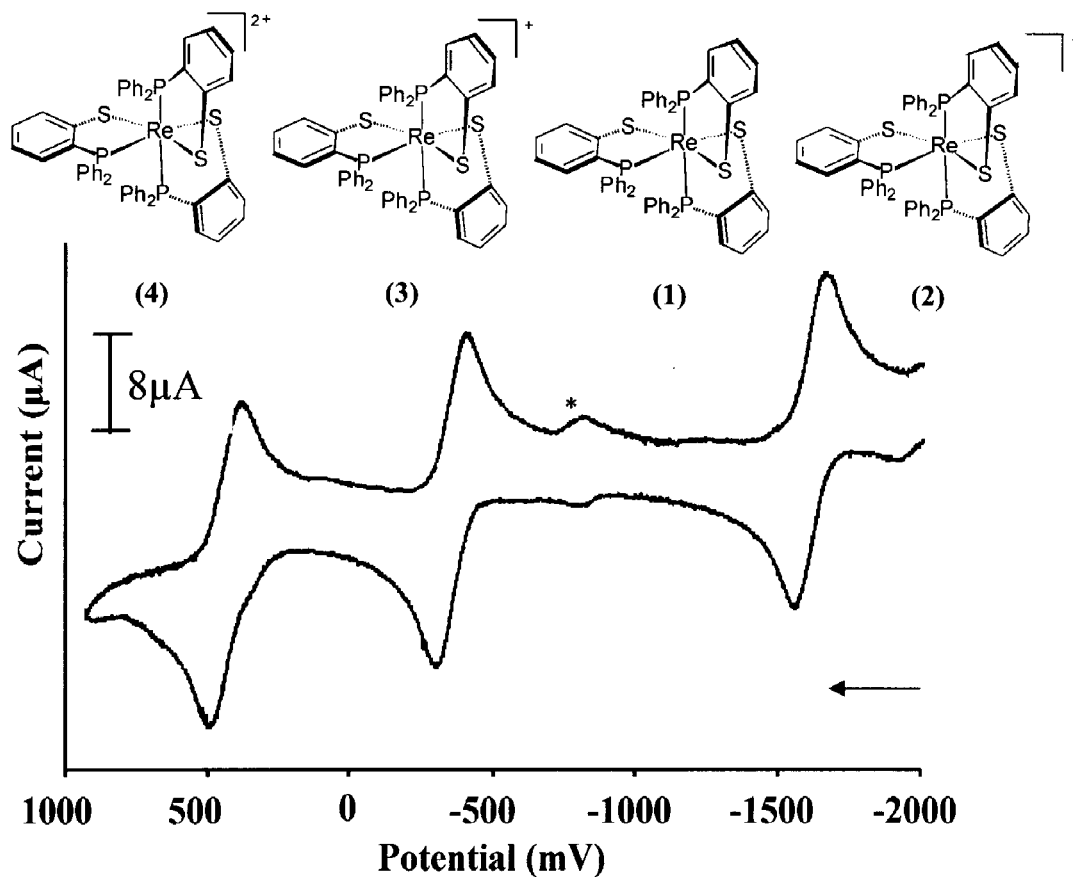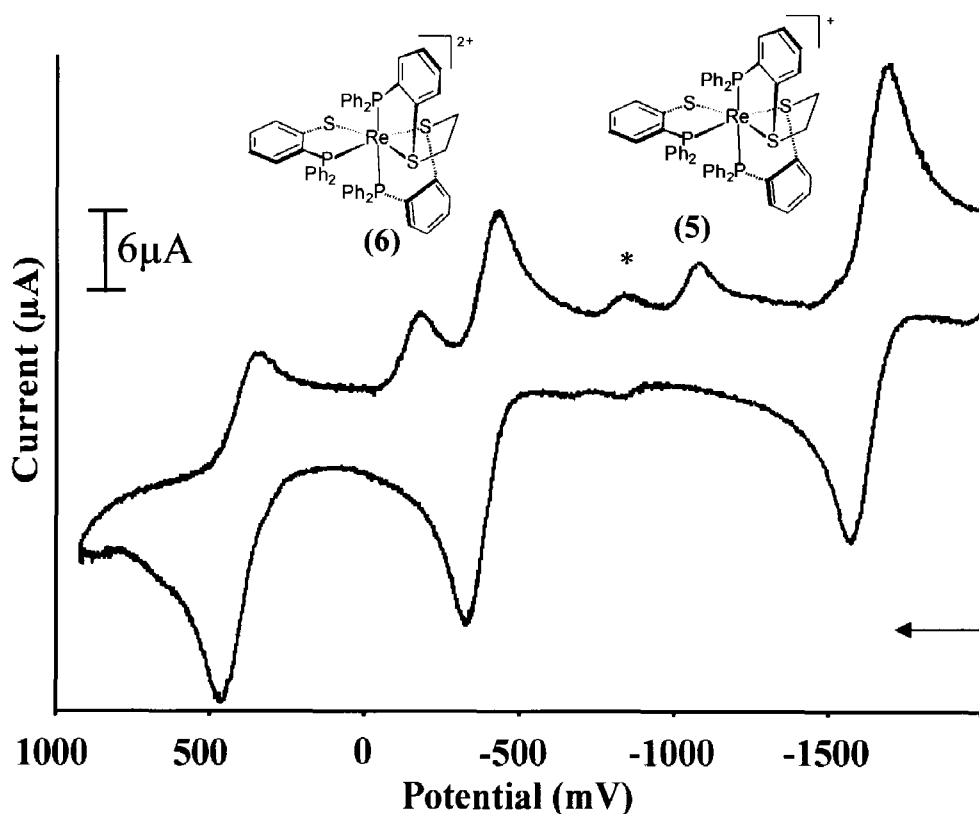
24

Figure III-2. Cyclic voltammogram of 1mM complex **(1)** obtained under ethylene atmosphere in dichloromethane at room temperature with 0.1 M TBAHFP as supporting electrolyte. The initial and final potentials were set to -2000mV with a switching potential of 1000mV. The initial potential was applied for 15 seconds before the scan. Potential referred to a ferrocenium/ferrocene reference (E_{obs} = +577mV). * is indicated as the impurity.

These new events are assigned as redox couples for the dithioether derivatives formed upon ethylene addition. The wave at -1010 mV (E_5) is assigned a Re(II)/Re(I) couple for the dithioether complexes **(5)/(8)**, and the wave at -100 mV (E_6) is assigned to the respective Re(III)/Re(II) of **(6)/(5)**. The **(6)/(5)** event shows current in both the anodic and cathodic scan, while the **(5)/(8)** couple only displays cathodic scan current. This is because ethylene does not add to the Re-thiolate until oxidation of **(1)** to **(3)** has occurred. The CV clearly shows the oxidation of **(1)** to **(3)** is unaffected by the presence of ethylene. Following that oxidation, **(3)** reacts with ethylene to form **(5)**. This reaction is not complete, and both the oxidation of **(5)** to **(6)** and the oxidation of unreacted **(3)** to **(4)**

25

are observed. The cathodic current for the **(6)/(5)** event exceeds the observed anodic current because **(3)**, and **(4)**, continue to react with ethylene as the scan continues. This is evident when 5 cycles are recorded as in Figure III-3.
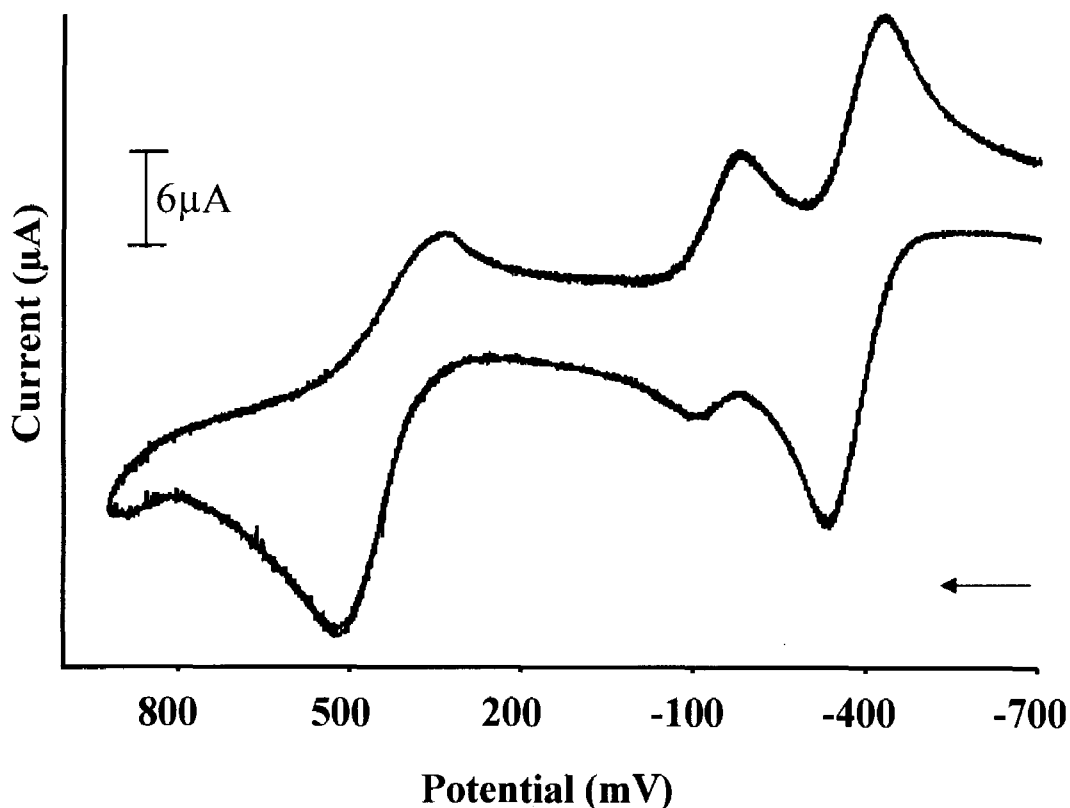
Figure III-3. Cyclic voltammogram of 1mM complex **(1)** obtained under ethylene atmosphere in dichloromethane at room temperature with 0.1 M TBAHFP as supporting electrolyte. The initial and final potentials were set to -700mV with a switching potential of 1000mV. The initial potential was applied for 15 seconds before the scan. Potential referred to a ferrocenium/ferrocene reference (E_{obs} = +577mV). This is 50 mV/s scan rate, and 5 cycles.

While **(1)** was unreactive with ethylene, oxidation initiates rapid C-S bond formation to yield **(5)** or **(6)** as a function of applied potential as described above. The formal Re (II) ion of **(5)** can be oxidized by one electron to Re(III) **(6)** (E_5 = -100 mV) or

reduced by one electron to Re(I) **(8)** (E$_4$ = -1010 mV). Reduction to **(8)** results in rapid ethylene loss and recovery of **(1)** suggesting K$_1$ ~ 0 is very small (see Scheme III-3).

Controlled potential bulk oxidation of **(1)** to **(3)** was accomplished by holding an applied potential of +23 mV in the spectroelectrochemical cell described in Chapter II. When the current decayed to 1-5% of the initial current, the oxidation process was considered complete. While the experimental time is dependent on the concentration and volume of the analyte and the quality of the working and counter electrode, 10 mL of 0.3 mM solution is typically oxidized (or reduced) completely after 400s. A plot of charge versus time for a typical oxidation of **(1)** to **(3)** under nitrogen is shown in Figure III-4.
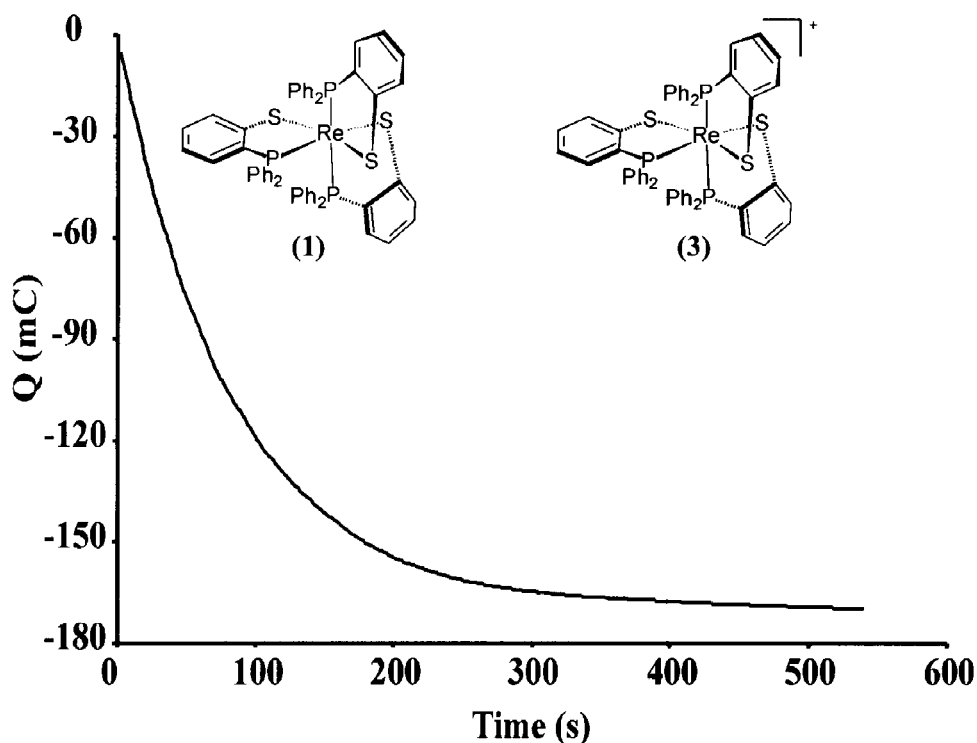

Figure III-4. A plot of charge versus time accomplished during the oxidation of **(1)** to **(3)** at low temperature.

The observed coulometric charge for the oxidation of (1) to (3) at 0.3 mM is -160

mC after correction for background current, which corresponds to 0.86 electron

equivalent (as per Faraday's law). Following oxidation, the square wave voltammogram

of (3) still shows three events at 427 mV, -357 mV and -1600 mV. These events are not

changed from those observed for (1) which indicates the coordination environment

around rhenium is not significantly changed upon oxidation, Figure III-5.
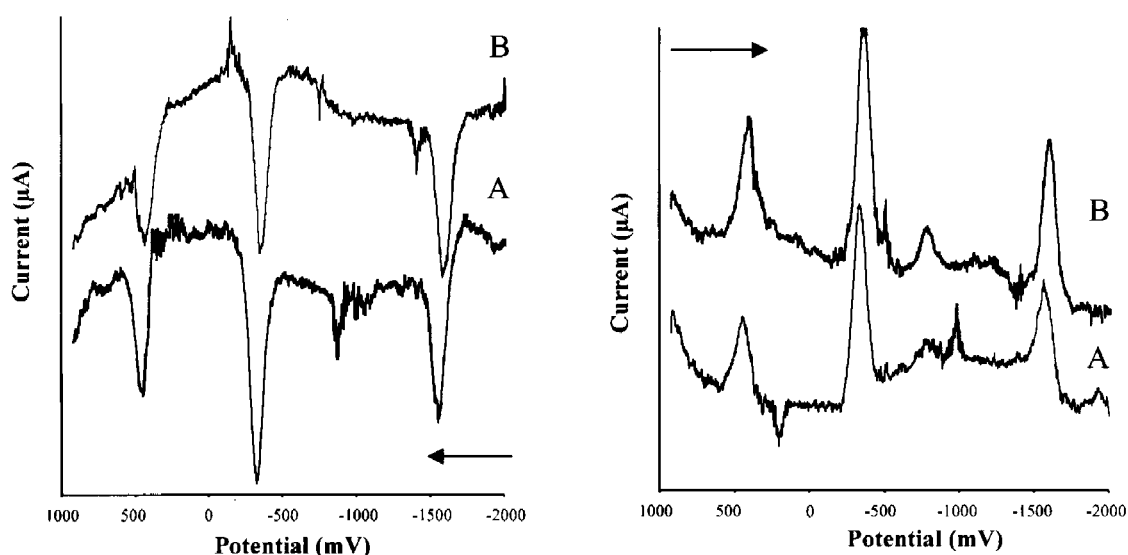
Figure III-5. Anodic (left) and cathodic (right) square wave voltammograms of (1) A and (3) B measured at low temperature versus an Ag pseudo reference electrode. Reported potentials are scaled to a ferrocenium/ferrocene reference (E_{obs} = +577 mV).

The oxidized complex (3) is blue in solution. A trace of the electronic spectra

recorded during oxidation of (1) to (3), Figure III-6, shows an intensity loss for the bands

at 329 nm and 535 nm associated with (1) and intensity gain for new bands at 390 nm and

581 nm associated with (3). Isosbestic points are observed at 368 nm and 551 nm.

Solutions of (3) are stable under nitrogen gas for several hours at room temperature.
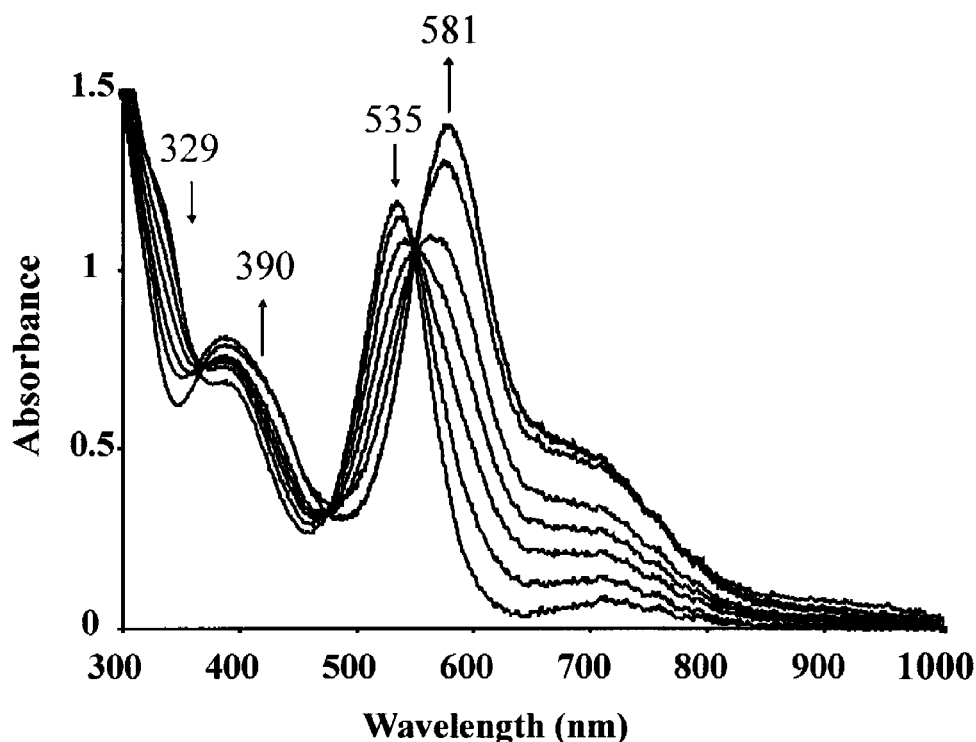
Figure III-6. Electronic spectra obtained during bulk oxidation of **(1)** to **(3)** under a nitrogen atmosphere at an applied potential of 23 mV. Data acquired approximately every 0.15 electron equivalents.

Fresh blue solutions of **(3)** were prepared by the electrochemical method mentioned above. Ethylene addition to blue solutions of **(3)** rapidly generates a purple solution containing a mixture of **(3)** and the addition product **(5)**, Figure III-7. Data was collected every 30 seconds for 10 minutes. The absorbance at 581 nm associated with **(3)** rapidly decreases from 2.14 to ~ 1.05 within 3 minutes of ethylene purging with no further significant changes thereafter. After 10 minutes, the solution was diluted to its original volume yielding an absorption value of 0.99 indicating an approximately ratio of **(3)**:**(5)** of 1:1.2. Assuming ethylene saturation of the solution (0.4642 M in CH_2Cl_2), K_2 is estimated as 2.5.

Consistent with equilibrium binding, the C-S bond of (5) can be easily cleaved by nitrogen purge within 10 minutes restoring the initial spectrum of (3), Figure III-8. A spectral trace was collected every 30 seconds. The C-S bond formation/cleavage cycle was repeated 7 times with no remarkable changes in efficiency, Figure III-9.
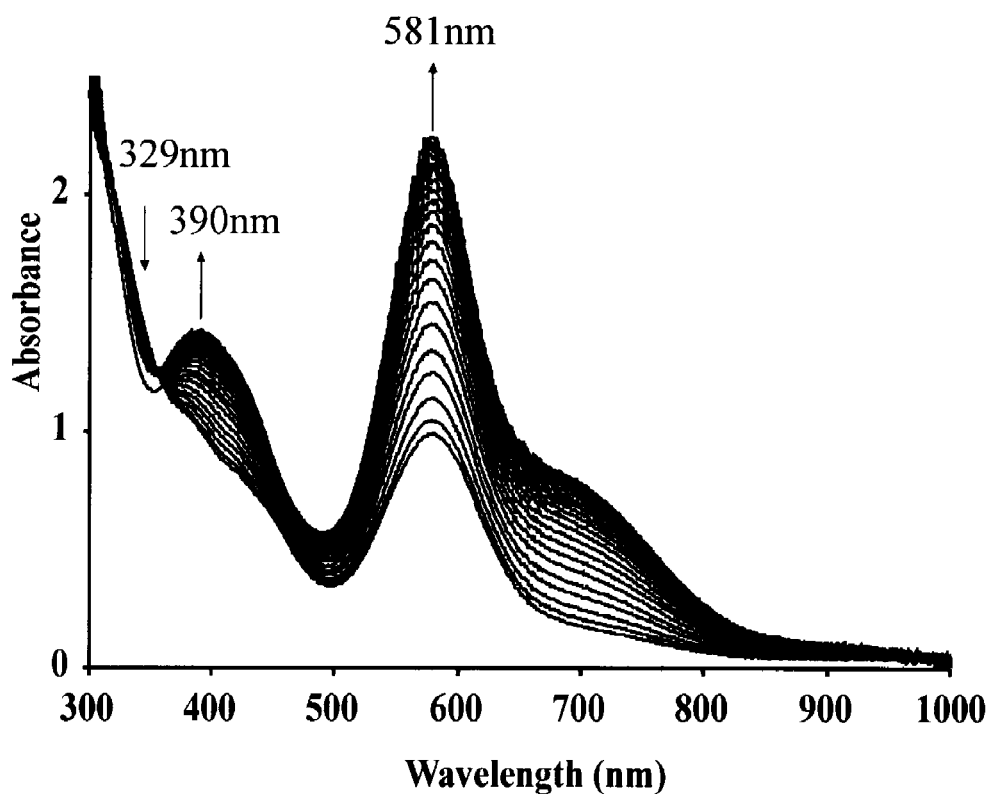
Figure III-8. Electronic spectra obtained during slow nitrogen purge through a solution of (5) at room temperature.
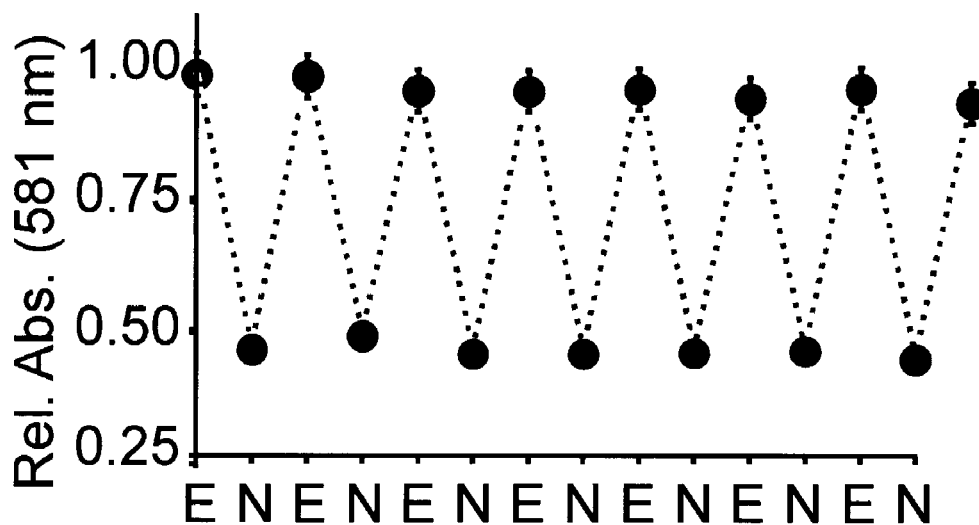
Figure III-9. The relative absorbance at 581 nm following alternating 10 minutes purges of ethylene (E) and nitrogen (N) are showing.

Carbon-sulfur bond cleavage can be thwarted by oxidation of (5) to (6), a formal Re(II) to Re(III) event. The requisite potential, E_5, lies slightly above E_2, but below E_3. Thus, solutions of (6) can be generated by bulk oxidation of (1) under an ethylene atmosphere via an ECE pathway. During bulk oxidation of (1) ($E_{applied}$ = +23 mV) under ethylene the color developed from blue to burgundy to purple to orange. UV-visible data recorded at -15°C in CH_2Cl_2 approximately every 0.15 electron equivalents reveals a two step process, Figure III-10. During the initial stage (1) is oxidized to (3), although the isosbestic points observed under nitrogen are obscured. During the second stage, (3) reacts with ethylene and is oxidized to (6) as indicated by the intensity loss at 390 and 581 nm and simultaneous intensity increase at 484 nm attributable to (6).
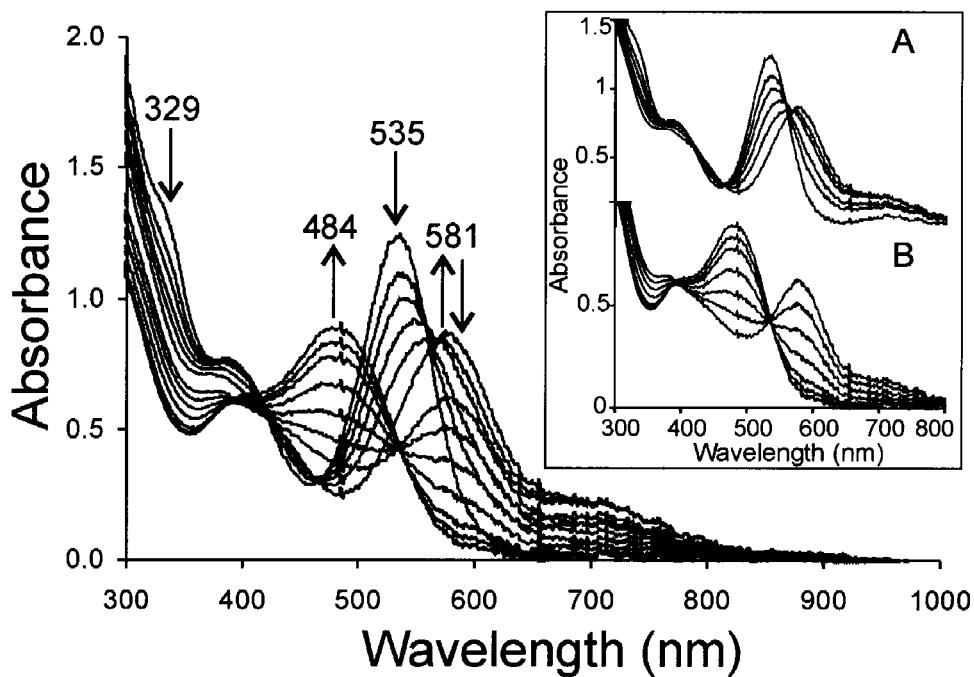
Figure III-10. Electronic spectra obtained during bulk oxidation of **(1)** to **(6)** under an ethylene atmosphere at an applied potential of +23 mV. Insets A and B highlight changes during the initial and latter stages of oxidation, respectively. Data acquired approximately every 0.15 equivalents.

The transferred total charge during oxidation of **(1)** under ethylene was experimentally determined to be -380 mC (1.94 electron equivalents). The progress of the bulk oxidation process was plotted as charge versus time in Figure III-11. This process was completed within 565 seconds.

32
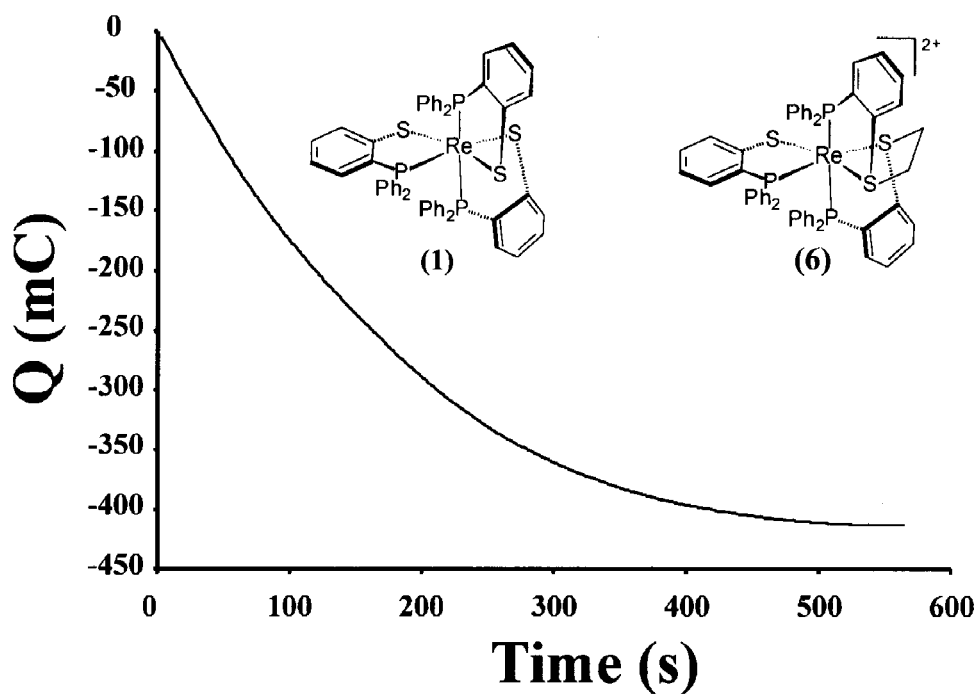
Figure III-11. A plot of charge versus time acquired during oxidation of **(1)** to **(6)** at low temperature.

Another preparation of **(6)** is performed by following ECE pathway. The complex **(1)** is oxidized for one electron to form the blue compound **(3)** under a nitrogen atmosphere at an applied potential of +23 mV. A trace of the UV-visible spectra recorded during the oxidation shows intensity gain at 390 and 581 nm. After the oxidation, this product was purged with ethylene for about 15 minutes to complete the chemical reaction to generate compound **(5)**, in equilibrium with **(3)**, as a purple solution. The electronic spectra recorded during this process shows intensity loss of 390 and 581nm and intensity gain at 329 nm. Then a potential of +23 mV was applied to the purple solution under ethylene purge. The coulometric total charge for this second step was measured as -160 mC which corresponds to 0.75 electron equivalent. The final product is compound **(6)** as

indicated by the orange color of the solution. The electronic spectra were shown in Figure III-12.
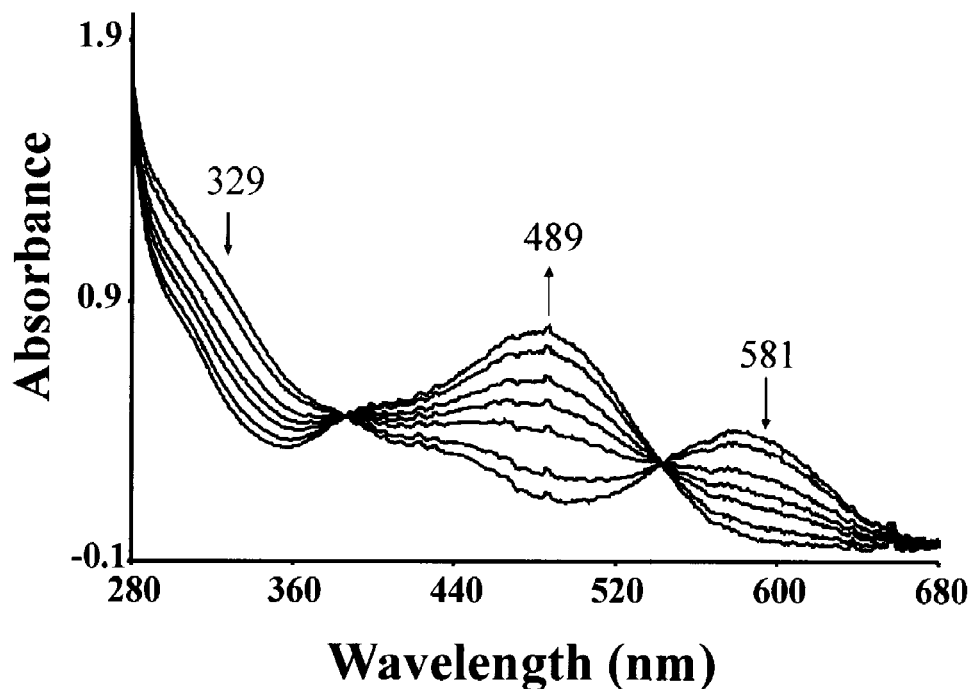
Figure III-12. Electronic spectra acquired during bulk oxidation **(5)** to **(6)** under ethylene atmosphere at an applied potential of +23 mV. Data recorded approximately every 0.15 electron equivalents.

A final alternate preparation of **(6)** was accomplished via an EEC pathway with oxidation of **(1)** by two electrons under nitrogen at an applied potential of 723 mV yielded **(4)**. This was followed by ethylene addition to yield **(6)**. These results were less satisfactory results as **(4)** decompose at a rate similar to ethylene addition (*vida infra*).

Although **(5)** adds ethylene reversibly, **(6)** does not undergo C-S bond cleavage in solution or in the solid state. No significant changes in the UV-visible spectrum of **(6)** are observed upon prolonged standing at room temperature for several hours, nitrogen purging and holding for two days, or exposure to vacuum via repeated cycles of freeze-

pump-thaw. C-S bond cleavage is only facilitated by reduction of (6) or (8). Figure III-13

displays square wave voltammograms of (6), recorded under ethylene atmosphere. The

potential window spans from +1000 mV to -2000 mV. Both cathodic and anodic scans

were evaluated with the initial potential held for 15 seconds prior to initiation of the scan.

Cathodic scans ($E_{initial}$ = +1000 mV) reveal events at -100, -1010, and -1620 mV assigned

as E_5, E_4, and E_1. Anodic scans ($E_{initial}$ = -2100 mV) show current associated with E_5, E_2,

and E_1. The results confirm rapid C-S bond cleavage at potentials less negative the

reduction of (5) to (8) and rapid C-S bond formation at potentials more positive than the

oxidation of (5) to (6). Additionally, the difference in formal Re (III)/ (II) reduction

potentials E_5 and E_1 of +1520 mV is consistent with the modification of two thiolate

donors in (1) to two thioether donors in (6). Importantly, reversible events were observed

for this result.[22,29,42,43]
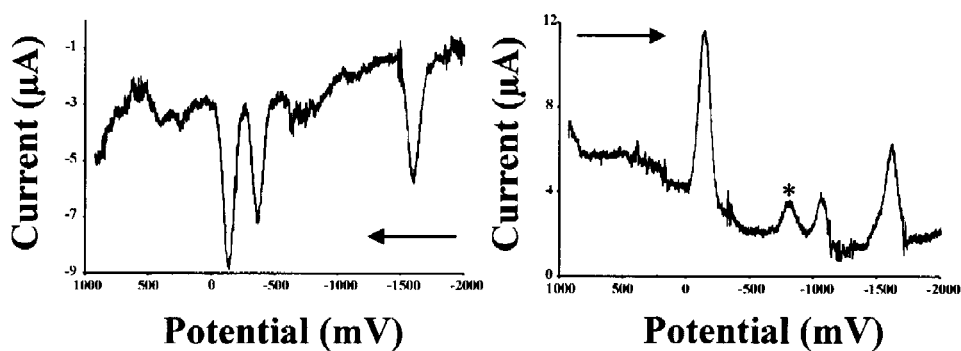
Figure III-13. Anodic (left) and cathodic (right) square wave voltammograms of (6) measured at low temperature versus an Ag pseudo-reference electrode. Reported potentials are scaled to ferrocenium/ferrocene reference (E_{obs} = +577 mV). * impurity due to partial decomposition.

As suggested by the square wave voltammograms, the ECE process for the formation of (6) from (1) and ethylene can be reversed upon bulk reduction. This was accomplished by applying a potential of -977 mV under a nitrogen purge. Figure III-14 displays a UV-visible trace recorded during the reduction.

In the first step of the reduction, the band associated with (6) at 484nm decreases while new bands for (3) increase at 390 and 581 nm. The second step is consistent with the further reduction of (3) to (1). The observed charge transferred the reduction was recorded at 365 mC (1.87 electron equivalents) and plotted as current versus time, Figure III-15.
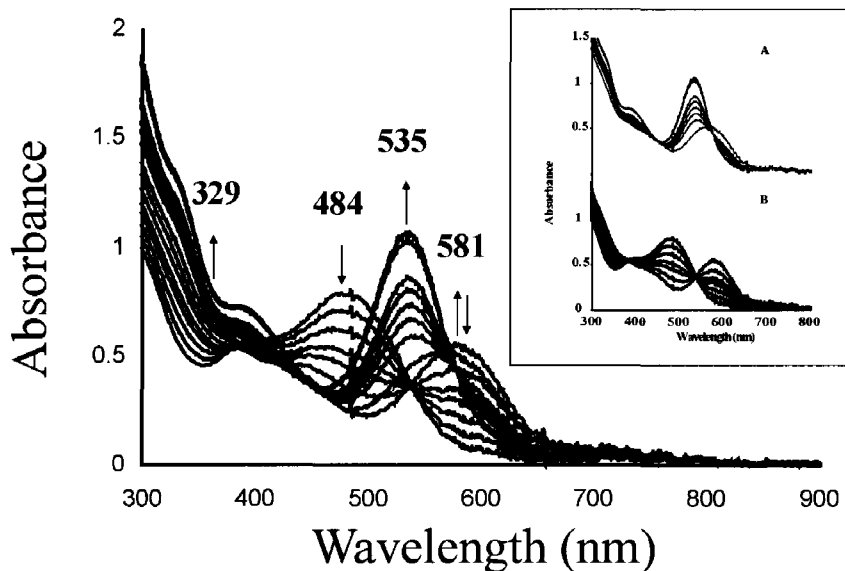
Figure III-14. Electronic spectra obtained during bulk reduction of (6) to (1) under a nitrogen atmosphere at an applied potential of -977 mV. Insets A and B highlight changes during the initial and latter stages of reduction, respectively.

36
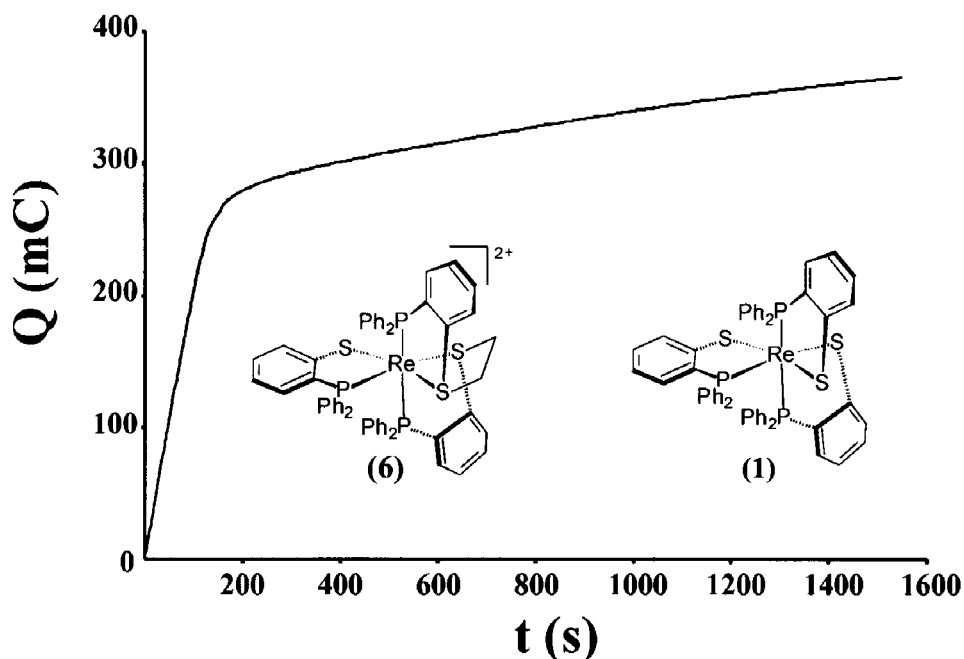
Figure III-15. A plot of charge versus time accomplished during reduction of **(6)** to **(1)** at low temperature.

The kinetic and equilibrium parameters associated with C-S bond formation/cleavage were extracted from cyclic voltammograms at multiple scan rates using the DigiSim software package.[34] The uncompensated resistance was estimated using the method at Bond *et al* as ~ 1.5 kΩ.[36] Simulation details and average fitting parameters are summarized in Table III-2.

Cyclic voltammograms recorded under nitrogen in a window from 1200 to -300 mV, Figure III-16 A, reveal a redox event identified as E_2 at -340 mV, which can be simulated as a single, reversible event. This single event is simulated as an E mechanism. Data collected under ethylene in window from 1200 to -300 mV, Figure III-16 B, display two additional events at -100 and -1010 mV assigned as E_5 and E_4, Figure III-16. As shown in the inset, the relative intensity of the new events increases at slower scan rates. These voltammograms were simulated with an ECEE mechanism.

Table III-2. Cyclic voltammetry simulation parameters

Table S1. Cyclic voltammetry simulation parameters

<u>Nitrogen Atmosphere; E Mechanism</u>

	E_2 (V)	α	k_s (cm/s)	D_o (cm²/s)	R_{uncomp} (Ω)
trial 1	-0.34	0.700	0.0780	3.48E-06	1500
trial 2	-0.33	0.700	0.0804	4.28E-06	1200
trial 3	-0.33	0.700	0.0792	4.07E-06	1300

<u>Ethylene Atmosphere; ECEE Mechanism</u>

	E_2 (V)	α	k_s (cm/s)	D_o (cm²/s)	R_{uncomp} (Ω)
trial 1	-0.34	0.700	0.0780	3.30E-06	1500
trial 2	-0.340	0.700	0.0800	5.07E-06	1200
trial 3	-0.35	0.700	0.0788	5.26E-06	1300

	E_5 (V)	α	k_s (cm/s)	D_o (cm²/s)	R_{uncomp} (Ω)
trial 1	-0.097	0.700	0.0943	3.30E-06	1500
trial 2	-0.097	0.700	0.0930	5.07E-06	1200
trial 3	-0.097	0.700	0.0934	5.26E-06	1300

	E_4 (V)	α	k_s (cm/s)	D_o (cm²/s)	R_{uncomp} (Ω)
trial 1	-1.00	0.700	0.0753	3.30E-06	1500
trial 2	-1.00	0.700	0.0737	5.07E-06	1200
trial 3	-1.00	0.700	0.0746	5.26E-06	1300

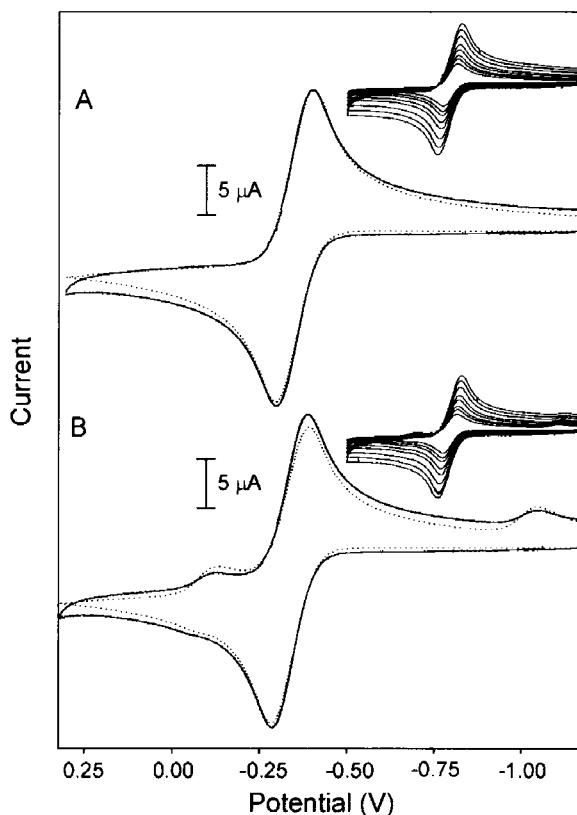|	K_2	k_f (M^{-1} s^{-1})	k_r (s^{-1})
trial 1	4.01	0.128	0.0318
trial 2	4.02	0.132	0.0328
trial 3	4.00	0.103	0.0259

Figure III-16. Experimental (−) and simulated (…) cyclic voltammograms of **(1)** small window under an atmosphere of nitrogen (A) or ethylene (B) at a scan rate of 200 mV/s. Insets show experimental voltammograms at multiple scan rates from 100 to 1000 mV/s.

Rate constant for C-S bond formation between **(3)** and ethylene, k_f, and for C-S bond cleavage for **(5)** were extracted from simulation of the CV data at 7 scan rates ranging from 100 to 1000mV/s for 3 independent trials. Average values for k_f and k_r are $(1.2 \pm 0.2) \times 10^{-1} \ M^{-1} \ s^{-1}$ and $(3.0 \pm 0.4) \times 10^{-2} \ s^{-1}$, respectively. From these, K_2 was calculated as 4.0 ± 0.8 in agreement with predictions from the UV-visible study. Under the pseudo-first conditions of ethylene saturation (0.4642 M), the apparent first-order of rate constants for ethylene addition to **(3)** is $(5.6 \pm 0.9) \times 10^{-2} \ s^{-1}$. Although ethylene addition to **(4)** was observed in cyclic voltammograms with a larger scan window,

attempts to determine reliable rate constants were hampered by decomposition of (4). The simulated and experimental events were shown in Figure III-17.
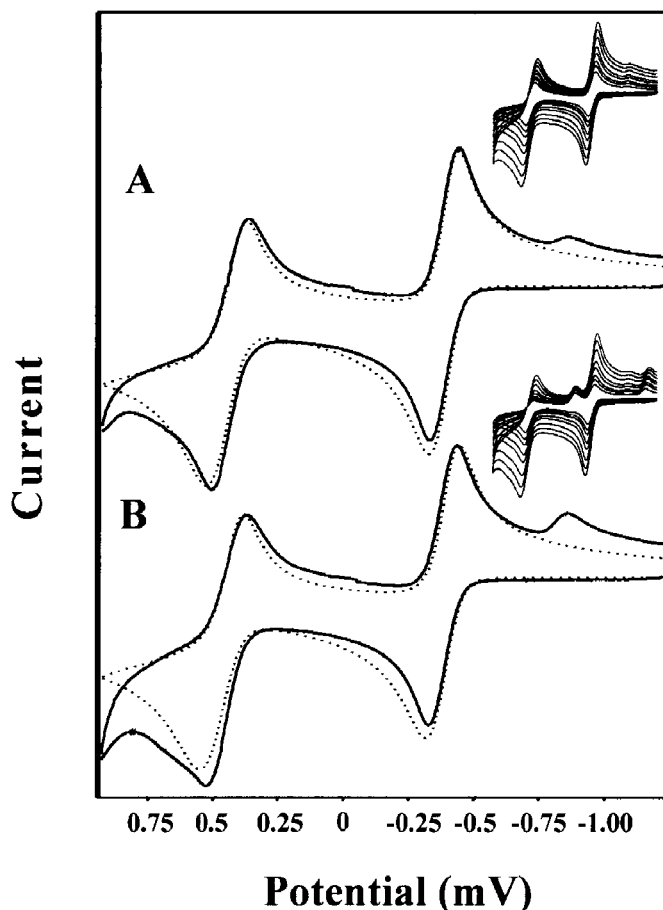
Figure III-17. Experimental (−) and simulated (...) cyclic voltammograms of (1) large window under a nitrogen atmosphere (A) and ethylene (B) at a scan rate of 200 mV/s. Insets show experimental voltammograms at multiple scan rates from 100 mV/s to 1000 mV/s.

From the redox potential E_2, E_3, E_4, and E_5 and the equilibrium constant K_2, values for K_1 and K_3 were determined.[44] K_1 has calculated value of $(1.9 \pm 0.4) \times 10^{-11}$ consistent with observation of an unstable C-S bond. In contrast, the calculated value of K_3, $(2.5 \pm 0.9) \times 10^9$, is large and consistent with the observed stability of (6). The large differences in equilibrium constants as a function of oxidation state provide a means to easily gate ethylene addition and release. In the most reduced form, (1)/(8), equilibrium

40

strongly favors the **(1)** and free ethylene. The ratio of the one electron oxidized pair **(3)/(5)** is a function of ethylene concentration and is approximately 1:2 in saturated solutions. Finally, the equilibrium of two electron oxidized pair **(4)/(6)** strongly favors **(6)** with tight ethylene binding.

In addition to electrochemical methods, **(6)** can be prepared by chemical oxidants via the ECE pathway. To solution of **(1)** in chlorobenzene was added $AgPF_6$ (2.0 equiv.) resulting in a rapid oxidation to **(3)** as observed by a blue color. Introduction of a slow ethylene purge for approximately five minutes followed by filtration to remove Ag(s) yields the desired product **(6)** as the hexafluorophosphate salt, as orange microcrystals. X-ray quality crystals were obtained by slow evaporation of a CH_2Cl_2/C_6H_5Cl solution of **(6)**. The (+)ESI-MS of crystalline **(6)** displays a parent peak at m/z = 547.0710 consistent with the expected value of 547.0766 and a smaller peak due to ethylene dissociation, at m/z = 533.0642 (z = 2) in agreement with the theoretical value of 533.0610, Figure III-18. From this characterization, the product identify of **(6)** is further confirmed.
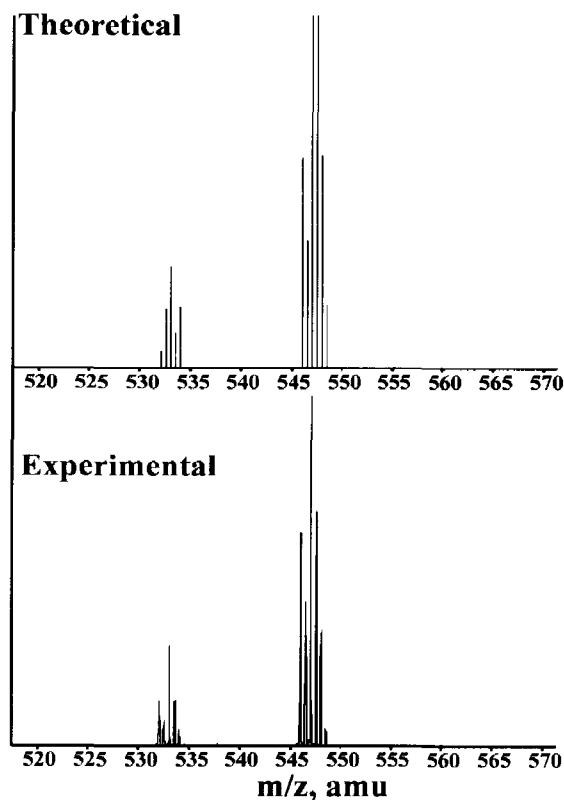
Figure III-18. (+)ESI-MS of (6).

The structure of (6) has been determined by single-crystal X-ray techniques.[45-52] The complex of (6) crystallizes as a long thin orange plate in the monoclinic space group C2/c with unit cell dimensions of a = 29.009(18) Å; b = 22.577(18) Å; c = 43.99(3) Å; β = 96.182(17)°, V = 28,643(35) Å³; D_{calc} = 1.413 Mg/m³, and Z = 8. An ORTEP representation of the rhenium containing cation of the asymmetric unit is shown in Figure III-19 with selected bond distances and angles provided in the figure caption.[53] The asymmetric unit of (6) contains two crystallographically independent cation molecules. All non-hydrogen atoms in both cations, as well as the hexafluorophosphate anions were refined with anisotropic atomic displacement parameters. The structural model has one full occupancy and three partial occupancy chlorobenzene solvate molecules.

42

The Re ion sits in pseudo-octahedral P_3S_3 donor arranged in an environment with phosphorus and sulfur donors arranged in a meridional fashion. The thioether sulfur donors S2 and S3 are bridged by the ethylene linker, while S1 is a thiolate donor. The Re-S thioether bond lengths for Re-S2 and Re-S3 are 2.434(3) Å and 2.432(3) Å, respectively, which are slightly longer than the Re-S thiolate bond lengths of 2.303(5) and of 2.269(5) Å in (1). To compensate shorter, the Re-S1 bond length is 2.209(3) Å and is slightly shorter than the value of Re-$S_{thiolate}$ of 2.477(5) Å in (1).[30] A similar trend is noted in the Re-P distances. The Re-P2 and Re-P3 in thioether bond lengths are 2.457(3) Å and 2.467(3) Å, respectively. Then the Re-P in a thiolate bond length is 2.420(3) Å. The C-C and C-S bonds associated with the ethylene bridge are consistent with single bond character with values of 1.491(14) Å, 1.864(11) Å and 1.831(10) Å for C(55)-C(56), S(2)-C(55), and S(3)-C(56), respectively. These values are very close to expected values for a C-C single bond.
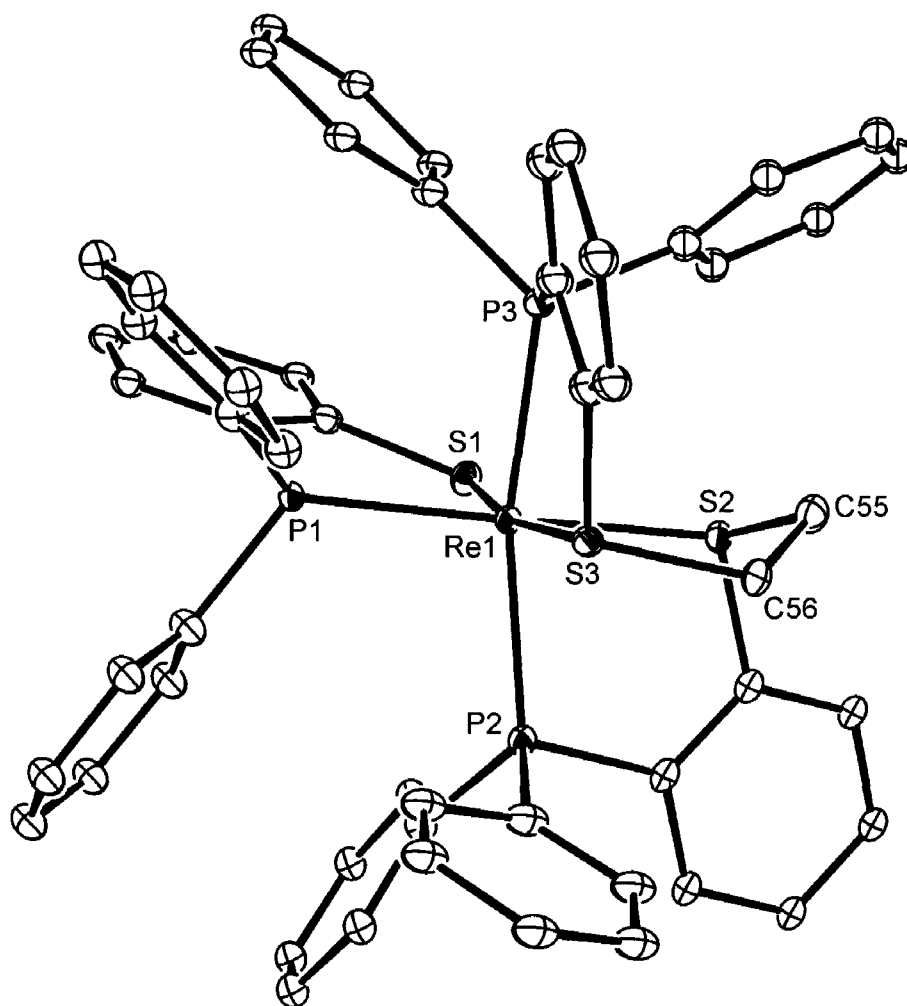
Figure III-19. ORTEP representation of **(6)**. Selected bond distances (Å): Re(1)-S(1) 2.209(3); Re(1)-S(2) 2.434(3); Re(1)-S(3) 2.432(3); Re(1)-P(1) 2.420(3); Re(1)-P(2) 2.457(3); Re(1)-P(3) 2.467(3); Selected bond angles (°): S(1)-Re(1)-S(3) 169.97(9); P(1)-Re(1)-S(2) 174.00(9); P(2)-Re(1)-P(3) 162.68(9); S(3)-Re(1)-S(2) 84.37(10).

The system described herein displays reversible C-S bond formation/cleavage regulated by the oxidation state of the complex with access to "locked on", "locked out", or concentration dependent ethylene addition. The kinetics of ethylene C-S formation/cleavage allows facile trap and release of ethylene over the period of several minutes.

CHAPTER IV

CONCLUSIONS
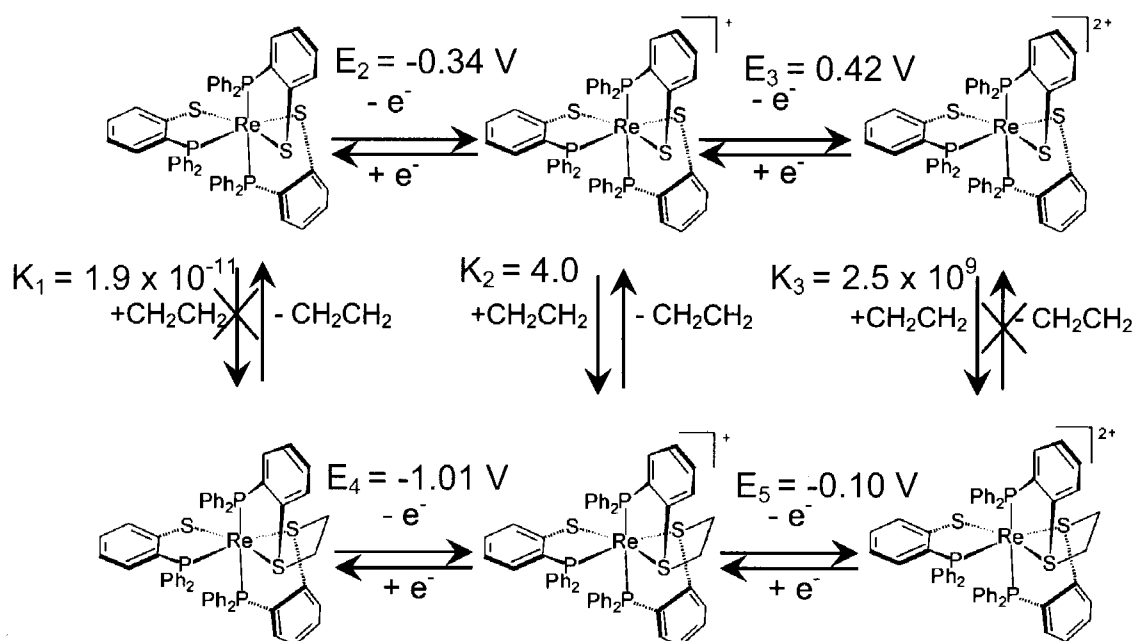
Scheme IV-1: Overview of ethylene addition.

In the study, we report reversible C-S bond formation/cleavage between ethylene and the rhenium derivative [Re(DPPBT)] **(1)** and its oxidized derivatives (Scheme IV-1). The equilibrium constants for ethylene binding are oxidation state dependent. The equilibrium constants were evaluated by cyclic voltammetric methods in ethylene saturated solution. The E_2 and E_4 were obtained from the experimental data and the equilibrium constant K_2 was defined by k_f and k_r from the simulation in the small window ECEE mechanism. Then the equilibrium constant K_1 was calculated as 1.9×10^{-11}

consistent with observation of an unstable C-S bond. This smaller value provides a mean to release ethylene; however, it is impossible to insert ethylene from the initial rhenium thiolates. In contrast, the calculated value of equilibrium constant K_3 was determined as 2.5×10^9 by E_3, E_5, and K_2 and this value is large regarded as the observed stablility of (6) complex. The C-S bond formation is strongly favored. The large difference in equilibrium constants as a function of oxidation state can be exploited as means to easily gate ethylene addition and release.

Alkene addition to oxidized metal-sulfur complexes has been previously reported, although a metal-coordinated thiyl radical was not invoked in the mechanism. Most notably, the addition of alkenes to nickel dithiolenes upon oxidation was reported by Stiefel and Wang in 2001. Then, reduction of the nickel dithiolene derived thioether resulted in alkene dissociation (Scheme I-4). This process was proposed to be of potentially great industrial importance in olefin purification.[10]

The electronic structure of the oxidized dithiolene complex was studied by Wieghardt and determined to be a diradical [Ni(II)(L$^{\cdot}$)$_2$], (L = dithiolene).[54] Upon introduction of an alkene, the diradical reacts resulting in C-S bond formation. In the reverse direction, controlled by switching the potential for a one electron reduction, C-S bond cleavage regenerates the original nickel complex and releases the alkene. However, later studies revealed the reactivity is more complex. Fekl and coworkers showed that the reactions of simple alkenes with nickel dithiolene do not proceed selectively to give the interligand alkene adduct. Competitive pathways leading to intraligand product interfere (Scheme I-4). The intraligand alkene adduct that is formed, further decomposes into dihydrodithiin and metal-decomposition products.[11]

For nickel dithiolenes, intraligand is preferred by symmetry.[54] As noted above and in Scheme IV-2, the electronic structure of nickel dithiolene has radical character. Further, alkene binding is dependent on the diradical ligand character of the Ni(II) complex. To prevent decomposition associated with the intraligand alkene adduct, we have used an alternate ligand as described in this thesis. The aromatic mixed thiol-phosphine ligand (DPPBTH = diphenylphosphinobenzenethiolate) has been reported, previously, together with a limited amount of their coordination chemistry.[31] The [Ru(DPPBT)$_3$]$^-$ complex was first studied by Dilworth *et al* as the HNEt$_3^+$salt.[55] The tri-thiolate ligand environment and an electron rich metal center makes it a suitable candidate to investigate metal versus ligand centered reactivity. The bulky ligand environment increases the possibility for radical stabilization. In the Grapperhaus group,
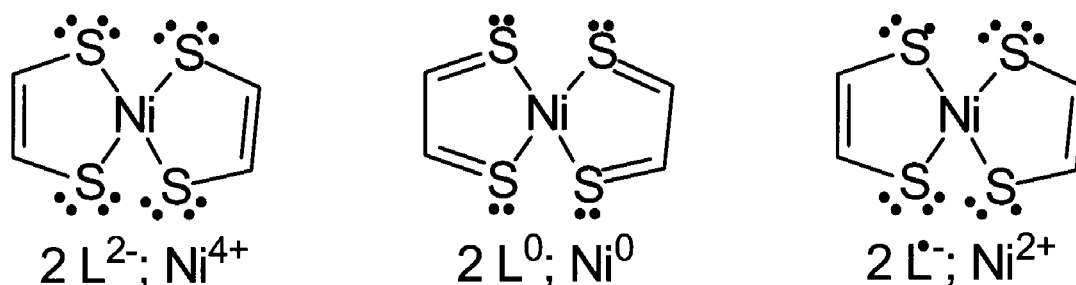
Scheme IV-2. Electronic structure of nickel-dithiolenes has radical character.

the HNEt$_3^+$ counter-ion of this complex was substituted with PPN$^+$ (PPN = bis(triphenylphosphoranylidene)ammonium) to improve the solubility.[22]

Previous results from our laboratory have shown that oxidation of [Ru(DPPBT)$_3$]$^-$ [1a]$^-$ proceeds in two one-electron steps.[29] Recent density functional theory (DFT)

investigations by Frye in the Grapperhaus group have determined the ground state of the

reactive intermediate $[Ru(DPPBT)_3]^+$. The ground state of $[Ru(DPPBT)_3]^+$ is best

considered as a singlet diradical, which is consistent with experimental data.[56] A

qualitative overview of the frontier molecular orbitals shows π interactions between Ru d-

orbitals and S p-orbitals in the xz, yz, and xy planes (Figure IV-1).
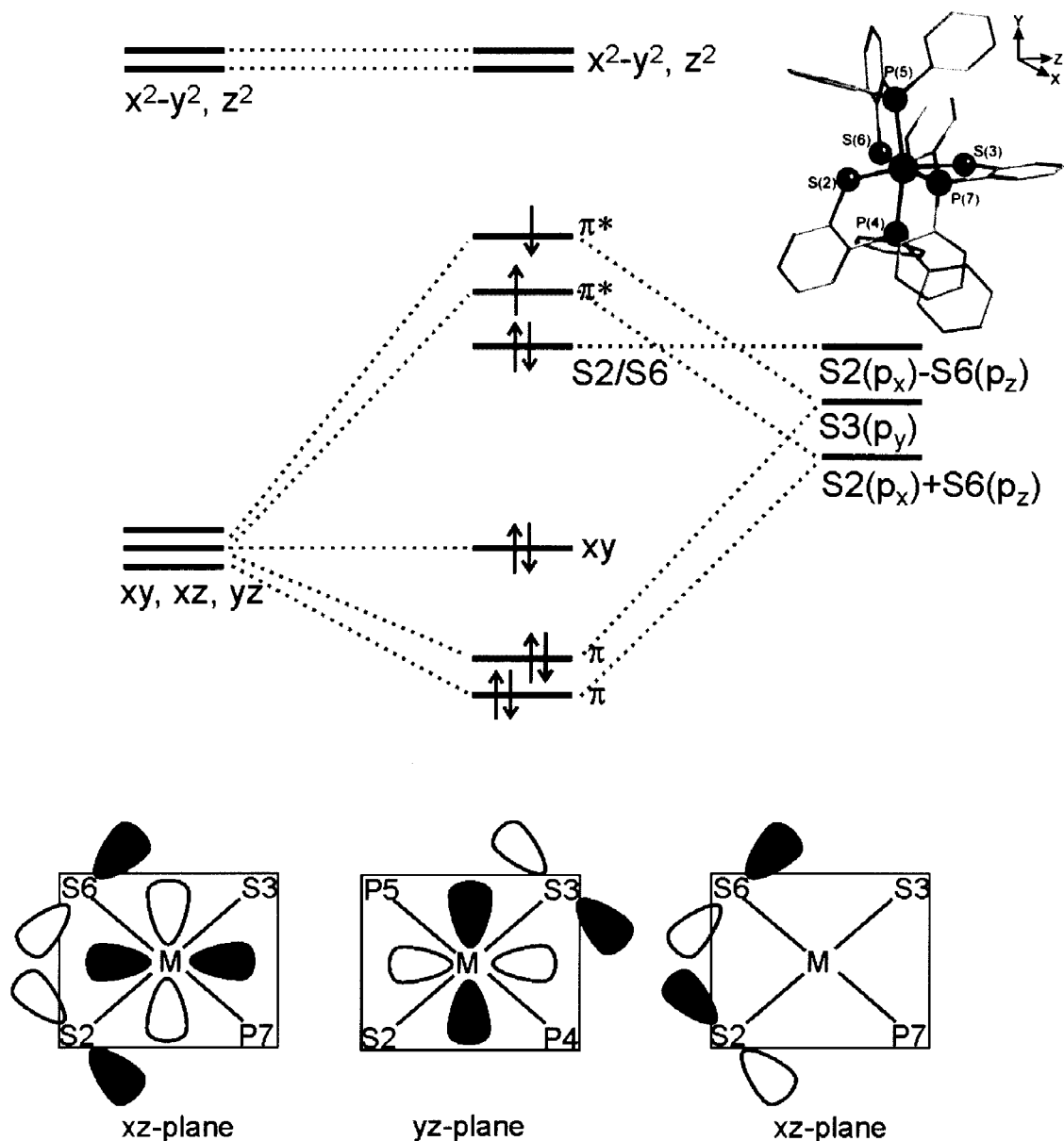
Figure IV-1. A qualitative overview of the frontier molecular orbitals shows π interactions between Ru d-orbitals and S p-orbitals in the xz, yz, and xy planes.

The configuration of ground state $[Ru(DPPBT)_3]^+$ is shown as $(S2(p_x) - S6(p_z))^2$, $(dxz - S2(p_x) - S6(p_z))^1$, and $(dxz - S3(p_y))^1$. This diradical ground state has unpaired electrons delocalized over the metal and sulfur donors in nearly orthogonal orbitals. Although $[Re(DPPBT)_3]$ and $[Ru(DPPBT)_3]^+$ are isoelectronic, addition of ethylene

proceeds for the ruthenium, but not the rhenium complex. This may be due to a lower

lying excited state of ruthenium that is reactive or a change in orbital ordering between

the two metals. Moreover, one oxidation of [Re(DPPBT)₃] results in C-S bond formation

and gives the expected configuration as $(S2(p_x) - S6(p_z))^1$, $(dxz - S2(p_x) - S6(p_z))^1$, and

$(dxz - S3(p_y))^1$. It is proposed that $[Re(DPPBT)_3]^+$ reacts with ethylene as shown in

Figure IV-2. The filled π*-orbital of sulfur reacts with LUMO empty π-orbital of C-C

double bond (Figure IV, left) and also vacant orbital of sulfur correlates with higher

orbital HOMO of π-bond alkene (Figure IV, right). C-S bond formation between ethylene

and the oxidized rhenium complex may be either stepwise or concerted mechanism. This

will be determined in further work.
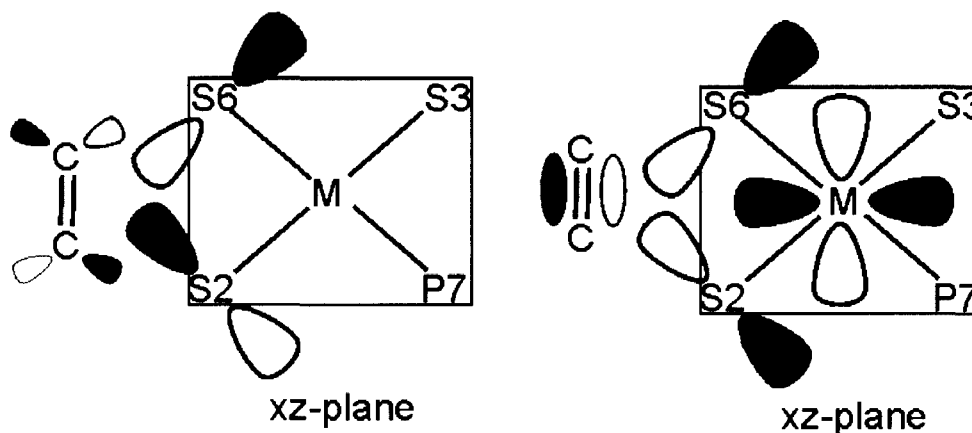
Figure IV-2. Views of the xz-planes highlighting interactions between S p orbitals and C-C bond orbitals.

Density Functional Theory (DFT) has been applied by Rothlisberger to

investigate the basis of C-S bond cleavage upon reduction of metal-thioethers. He found

that C-S bond breaking requires donation of two electrons from a metal t_{2g}-orbital into the

π-bond of the departing ethylene. The relative energies of the frontier orbitals for the

metal-thioether reactant (left of each panel) and the metal thiolate product (right of each panel) and the π-bonding orbital of ethylene (denoted with a *) is shown as in Figure IV-3.[40]
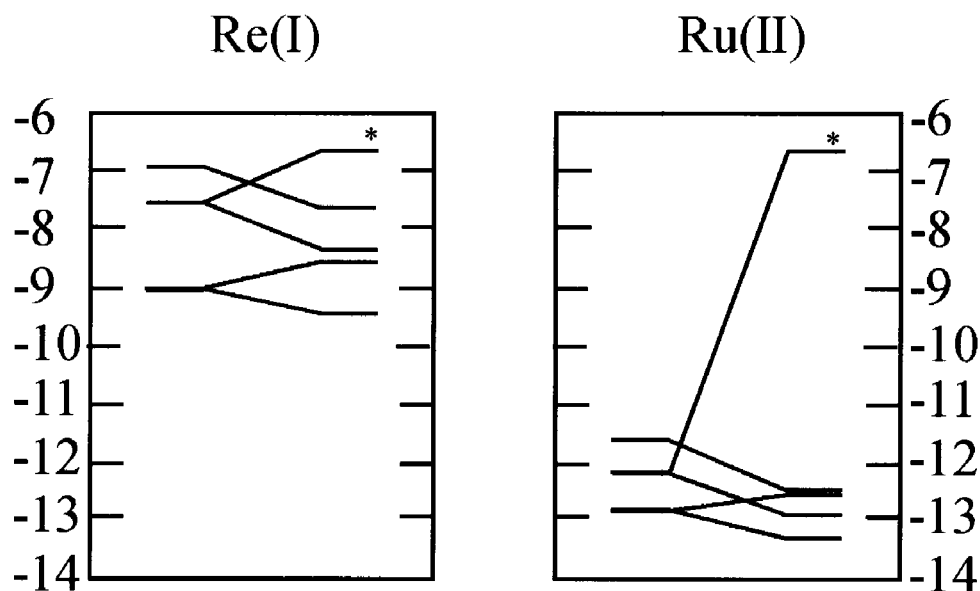
Figure IV-3. Eigenvalues (eV) of five highest molecular orbitals of the metal-thioether complex for Re(I)-thioether and Ru(II)-thioether on the left side of each panel and the metal-thiolate complex for Re(III)-thiolate and Ru(IV)-thiolate on the right side of each panel are obtained. A * represents π-bonding orbital of ethylene.

The left side of each panel shows the five highest occupied molecular orbitals of the metal-thioether complex for a Re (I)-thioether. The top three orbitals are based on the metal t_{2g} orbitals and the bottom two orbitals consist of sulfur lone pairs. The right side of each panel represents the Re(III)-thiolate and Ru(IV)-thiolate orbital energies plus an orbital marked with a * for the π-bonding orbital of ethylene. Rapid C-S bond cleavage for Re (I)-thioethers can occur because there is no significant energy difference between the higher energy of metal t_{2g} orbitals and the π-bonding orbital of ethylene. However, the

more positive charge of Ru (II) lowers the energy of the t_{2g}-orbital in the other case. As a result there is no energy match between metal orbitals and π-bonding orbital of ethylene. This makes the Ru (II)-thioether complex more stable than Re (I)-thioether complex. Overall, the main factor governing the reaction energy is the overall charge of the complex.

Reversible carbon-sulfur bond formation/cleavage between a rhenium-thiolate complex and ethylene was reported in Chapter III. By regulation of the oxidation state and therefore the charge of the complex, the affinity of the complex for ethylene can be tuned. The ethylene can be "locked on" in the higher oxidation state or "locked off" in the lower oxidation state. Ethylene binding to the intermediate oxidation state is concentration dependent, Scheme IV-3.
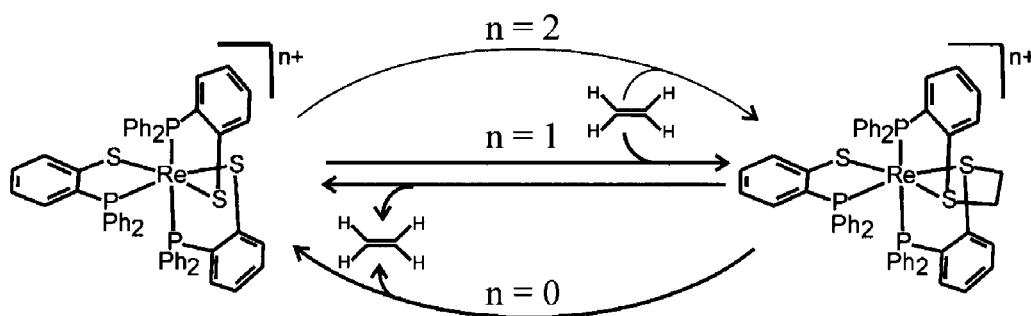
Scheme IV-3. Reversible C-S bond formation/cleavage between **(1)**, **(8)**, and oxidized derivatives.

The results are consistent with the theoretical prediction of Rothlisberger. The original rhenium (III) trithiolate complex **(1)** is oxidized in one electron step at applied potentials of $+23$ mV and 723 mV during the bulk electrolysis, providing rhenium (IV) **(3)** and rhenium (V) **(4)**, respectively. These products in higher oxidation state eventually

react with ethylene to obtain thioether complexes. Upon reduction, the C-S bond cleaves immediately.

Past investigations the Grapperhaus group revealed that an oxidized ruthenium thiolate formed a carbon-sulfur bond with alkenes including 1-hexene, styrene, cyclohexene, and norbornene as shown in Scheme IV-4. In the future directions, bulkier alkenes will be investigated with referred to their addition to rhenium. Moreover, the selectivity of alkenes and the binding mechanism, whether concerted or stepwise, will be further determined.

For the nickel dithiolene complex reported by Stiefel and Wang, the oxidized reactive species were reported not be poisoned by gases including hydrogen, carbon monoxide, acetylene, or hydrogen sulfide. These gases are important contaminants that must be removed industrially during olefin purification. These potentially reactive gases will also be investigated for the rhenium thiolate system reported in this thesis.
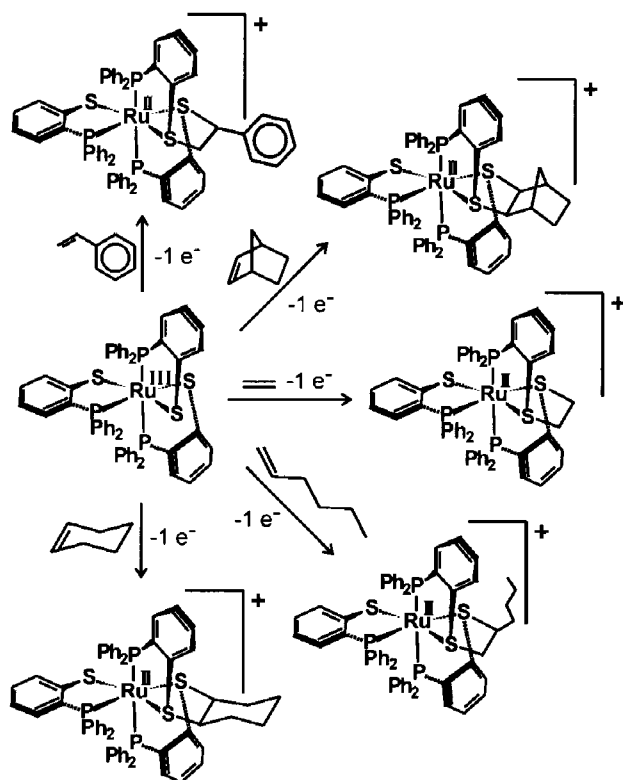
Scheme IV-4. [Ru(DPPBT)₃] reacts with various alkenes to yield respective Ru (II)-dithioether compounds.

REFERENCES

1.   http://en.wikipedia.org/wiki/Ethylene

2.   *Chem. Eng. News* June 28, 1999, pp 34-35.

3.   *Chem. Eng. News* July 7, 2008, pp 61-69.

4.   "Ethylene". In *in Kirk-Othmer concise encyclopedia of chemical technology*, Howe-Grant, M., Ed. Wiley: New York, **1999**.

5.   Mark, F. H., Othmer, F. D., Overberger, C. G., Seaborg, T. G. In *Encyclopedia of Chemical Technology*, 3rd ed.; John Wiley & Sonc, Inc.: New York, 1978; Vol. 9.

6.   Grantom, L. R., Royer, J. D. In *Ull-mann's Encyclopedia of Industrial Chemistry*, 5th ed.; VCH: New York, **1987**; pp 45-93.

7.   Suzuki, T.; Noble, R. D.; Koval, C. A. Electrochemistry, Stability, and Alkene Complexation Chemistry of Copper(I) Triflate in Aqueous Solution. Potential for Use in Electrochemically Modulated Complexation-Based Separation Processes. *Inorg. Chem.* **1997**, *36*, 136-140.

8.   Rodríguez, F. I.; Esch, J. J.; Hall, A. E.; Binder, B. M.; Schaller, G. E.; Bleecker, A. B. A Copper Cofactor for the Ethylene Receptor ETR1 from Arabidopsis. *Science* **1999**, *283*, 996-998.

9.   McKenna, M.; Wright, L. L.; Miller, D. J.; Tanner, L.; Haltiwanger, R. C.; DuBois, M. R. Synthesis of inequivalently bridged cyclopentadienyl dimers of molybdenum and a comparison of their reactivities with unsaturated molecules and with hydrogen. *J. Am. Chem. Soc.* **1983**, *105*, 5329-5337.

10.   Wang, K.; Stiefel, E. I. Toward Separation and Purification of Olefins Using Dithiolene Complexes: An Electrochemical Approach. *Science* **2001**, *291*, 106-109.

11.   Harrison, D. J.; Nguyen, N.; Lough, A. J.; Fekl, U. New Insight into Reactions of $Ni(S_2C_2(CF_3)_2)_2$ with Simple Alkenes: Alkene Adduct versus Dihydrodithiin Product Selectivity Is Controlled by $[Ni(S_2C_2(CF_3)_2)_2]^-$ Anion. *J. Am. Chem. Soc.* **2006**, *128*, 11026-11027.

12.   Geiger, W. E. Electrochemistry of Cycloaddition Products of Olefins with Nickel Dithiolenes: A Reinvestigation of the Reduction of the 1:1 Adduct between $Ni(S_2C_2(CF_3)_2)_2$ and Norbornadiene. *Inorg. Chem.* **2002**, *41*, 136-139.

13.   Jantz, D.; Amann, B. T.; Gatto, G. J.; Berg, J. M. The Design of Functional DNA-Binding Proteins Based on Zinc Finger Domains. *Chem. Rev.* **2004**, *104*, 789-800.

14.   Matthews, R. G.; Goulding, C. W. Enzyme-catalyzed methyl transfers to thiols: the role of zinc. *Curr. Opin. Chem. Biol.* **1997**, *1*, 332-339.

15.   Cammack, R. *"Iron-Sulfur Clusters in Enzymes: Themes and Variations"*. **1992**; Vol. 38, p 281-322 and reference therein.

16.   Grapperhaus, C. A.; Mullins, C. S.; Kozlowski, P. M.; Mashuta, M. S. Synthesis and Oxygenation of a Nickel(II) and Zinc(II) Dithiolate: An Experimental and Theoretical Comparison. *Inorg. Chem.* **2004**, *43*, 2859-2866.

17.   Ashby, M. T.; Enemark, J. H.; Lichtenberger, D. L. Destabilizing d.π.-p.π. orbital interactions and the alkylation reactions of iron(II)-thiolate complexes. *Inorg. Chem.* **1988**, *27*, 191-197.

18.   *"S-centered radicals"*. John Wiley & Sons: Chichester, **1999**.

19.   Walling, C.; Helmreich, W. Reactivity and Reversibility in the Reaction of Thiyl Radicals with Olefins. *J. Am. Chem. Soc.* **1959**, *81*, 1144-1148.

20.   Ichinose, Y., Oshima, K., Utimoto, K. Application of Free Radical Substitution Reaction into Interconversion of 1-Alkenylsulfides, 1-Alkenylgermanes, and 1-Alkenylstannanes. *Chem. Lett.* **1988**, *17*, 669-672.

21.   Huheey, E. J. *"Inorganic Chemistry"*. 3rd ed.; Harper & Row: New York, **1983**.

22.   Grapperhaus, C. A.; Poturovic, S.; Mashuta, M. S. Dichloromethane Alkylates a Trithiolato-Ruthenium Complex to Yield a Methylene-Bridged Thioether Core. Synthesis and Structural Comparison to the Thiolato-Ruthenium Precursor. *Inorg. Chem.* **2002**, *41*, 4309-4311.

23.   Kimura, S.; Bill, E.; Bothe, E.; Weyhermuller, T.; Wieghardt, K. Phenylthiyl Radical Complexes of Gallium(III), Iron(III), and Cobalt(III) and Comparison with Their Phenoxyl Analogues. *J. Am. Chem. Soc.* **2001**, *123*, 6025-6039.

24.   Ghosh, P.; Bill, E.; Weyhermuller, T.; Neese, F.; Wieghardt, K. Noninnocence of the Ligand Glyoxal-bis(2-mercaptoanil). The Electronic Structures of $[Fe(gma)]_2$, $[Fe(gma)(py)].py$, $[Fe(gma)(CN)]^{1-/0}$, $[Fe(gma)I]$, and $[Fe(gma)(PR_3)_n]$ (n = 1, 2). Experimental and Theoretical Evidence for "Excited State" Coordination. *J. Am. Chem. Soc.* **2003**, *125*, 1293-1308.

25. Herebian, D.; Bothe, E.; Bill, E.; Weyhermuller, T.; Wieghardt, K. Experimental Evidence for the Noninnocence of o-Aminothiophenolates: Coordination Chemistry of o-Iminothionebenzosemiquinonate(1-) π-Radicals with Ni(II), Pd(II), Pt(II). *J. Am. Chem. Soc.* **2001,** *123,* 10012-10023.

26. Hsieh, C. H.; Hsu, I. J.; Lee, C. M.; Ke, S. C.; Wang, T. Y.; Lee, G. H.; Wang, Y.; Chen, J. M.; Lee, J. F.; Liaw, W. F. Nickel Complexes of o-Amidochalcogenophenolate(2-)/o-Iminochalcogenobenzosemiquinonate(1-) π-Radical: Synthesis, Structures, Electron Spin Resonance, and X-ray Absorption Spectroscopic Evidence. *Inorg. Chem.* **2003,** *42,* 3925-3933.

27. Grapperhaus, C. A.; Poturovic, S. Electrochemical Investigations of the [Tris(2-(diphenylphosphino)thiaphenolato)ruthenate(II)] Monoanion Reveal Metal- and Ligand-Centered Events: Radical, Reactivity, and Rate. *Inorg. Chem.* **2004,** *43,* 3292-3298.

28. Poturovic, S., Mashuta, S.M., Grapperhaus, C. A. Carbon-Sulfur Bond Formation between a Ruthenium-Coordinated Thiyl Radical and Methyl Ketones. *Angew. Chem. Int. Ed.* **2005,** *44,* 1883-1887.

29. Grapperhaus, C. A.; Venna, K. B.; Mashuta, M. S. Carbon-Sulfur Bond Formation via Alkene Addition to an Oxidized Ruthenium Thiolate. *Inorg. Chem.* **2007,** *46,* 8044-8050.

30. Dilworth, J. R., Huston, A. J., Morton, S., Harman, M., Hursthouse, M. B., Zubieta, J., Archer, C. M., Kelly, J. D. "The preparation and Electrochemistry of Technetium and Rhenium Complexes of 2-(diphenylphosphino)benzenethiol. The Crystal and Molecular Structures of [Re(2-Ph$_2$PC$_6$H$_4$S$_3$)$_3$] and [Tc(2-Ph$_2$PC$_6$H$_4$S$_3$)$_3$]". *Polyhedron* **1992,** *11,* 2151-2155.

31. Block, E.; Ofori-Okai, G.; Zubieta, J. 2-Phosphino- and 2-phosphinylbenzenethiols: new ligand types. *J. Am. Chem. Soc.* **1989,** *111,* 2327-2329.

32. John, N. P., Lock, C. J., Wilkinson, G. Amine, Phosphine, Arsine, and Stibine Complexes of Rhenium-(III), -(IV), and -(V). *J. Chem. Soc.* **1964,** 1054-1066.

33. Gordon, A. J. *"The Chemistry Companion".* John Wiley & Sons Inc.: Canada, **1972.**

34. Rudolph, M., Feldberg, S. W. *"DigiSim",* Bioanalytical Systems, Inc.: West Lafayette, IN, 2004.

35. www.epsison-web.net/Ec/digisim/tutorials/tut_2.html

36. Bond, A. M.; Oldham, K. B.; Snook, G. A. Use of the Ferrocene Oxidation Process To Provide Both Reference Electrode Potential Calibration and a Simple Measurement (via Semiintegration) of the Uncompensated Resistance in Cyclic

Voltammetric Studies in High-Resistance Organic Solvents. *Anal. Chem.* **2000,** *72*, 3492-3496.

37.   Kissinger, P. T., Heineman, W. R. "Instrumentional Examples of Electrodes Mechanisms of Transition Metal Complexes". In *In Laboratory Techniques in Electroanalytical Chemistry*, 2nd ed.; Marcel Dekker, Inc.: New York, **1996,** pp 695-697.

38.   Bard, J. A., Faulkner, R. L. *"Electrochemical Methods: Fundamentals and Applications".* 2nd ed.; John Wiley & Sons, Inc.: 2001.

39.   Wasserscheid, P.; Hilgers, C.; Keim, W. Ionic liquids--weakly-coordinating solvents for the biphasic ethylene oligomerization to [alpha]-olefins using cationic Ni-complexes. *J. Mol. Catal. A: Chem.* **2004,** *214*, 83-90.

40.   Maurer, P.; Magistrato, A.; Rothlisberger, U. Theoretical Studies of the Reductive C-S Bond Cleavage in Complexes of the Form $[M(9S3)_2]^{2+}$ (M = Re, Tc, and Ru; 9S3 = 1,4,7-Trithiacyclononane). *J. Phys. Chem. A* **2004,** *108*, 11494-11499.

41.   Magistrato, A.; Maurer, P.; Fassler, T.; Rothlisberger, U. First-Principles Simulations of C-S Bond Cleavage in Rhenium Thioether Complexes. *J. Phys. Chem. A* **2004,** *108*, 2008-2013.

42.   Grapperhaus, C. A.; Mullins, C. S.; Mashuta, M. S. Structural comparison of alkylated derivatives of (bmmp-dmed)Ni and (bmmp-dmed)Zn. *Inorg. Chim. Acta* **2005,** *358*, 623-632.

43.   Farmer, P. J.; Reibenspies, J. H.; Lindahl, P. A.; Darensbourg, M. Y. Effects of sulfur site modification on the redox potentials of derivatives of [N,N'-bis(2-mercaptoethyl)-1,5-diazacyclooctanato]nickel(II). *J. Am. Chem. Soc.* **1993,** *115*, 4665-4674.

44.   Miller, S. R.; Gustowski, D. A.; Chen, Z. H.; Gokel, G. W.; Echegoyen, L.; Kaifer, A. E. Rationalization of the unusual electrochemical behavior observed in lariat ethers and other reducible macrocyclic systems. *Anal. Chem.* **1988,** *60*, 2021-2024.

45.   *SHELXTL. (v6.14), Program Library for Structure Solution and Molecular Graphics*, Brucker Advanced X-ray Solution, Inc.: Madison, WI, 2000.

46.   *SAINT (V.6.45a)*, Brucker Advanced X-ray Solutions, Inc.: Madison, WI, **2003**.

47.   *SMART(v.5632)*, Brucker Advanced X-ray Solutions, Inc.: Madison, WI, **2005**.

48.   Sheldrich, M. G. SHELXS-90. *Acta Crystallogr.* **1990**, A46-467.

49.   Sheldrich, M. G. SHELXL-97. *Program for the Refinement of Crystal Structures.* In Univeristy Gottingen: Gottingen, Germany, **1997**.

50. Sheldrich, M. G. *SADABS (V.2.10), Area Detector Absorption Correction*, University Gottingen: Gottingen, Germany, **2003**.

51. Crystal data for (**7**): orange needles, m., space group C2/c, a = 29.009(18) Å, b = 22.577(18) Å, c = 43.99(3) Å, β = 96.182(17) °, V = 28643(35) Å^3, ρ_{calcd} = 1.413 g/cm^3, Z = 8. Data were collected on a Brucker SMART APEX CCD using Mo$_{k\alpha}$ radiation. For all 25546 unique reflections (R(int) = 0.073), the final anisotropic full-matrix least-squares refinement on F^2 for 1282 variables converged at R1 = 0.125, wR2 = 0.184 with a GOF of 1.09. CCDC-699464 contains the supplementary crystallographic data for this paper. Data can be obtained free of charge from The Cambridge Crystallographic Data Center via www.ccdc.cam.ac.uk/data_request.cif.

52. Spek, L. A. *SQUEEZE*, University of Utrecht: Utrecht, The Netherlands, **1992**.

53. Farrugia, J. L. *J. Appl. Crystallogr.* **1997**, *30*, 565.

54. Ray, K.; Weyhermuller, T.; Neese, F.; Wieghardt, K. Electronic Structure of Square Planar Bis(benzene-1,2-dithiolato)metal Complexes [M(L)$_2$]^z (z = 2-, 1-, 0; M = Ni, Pd, Pt, Cu, Au): An Experimental, Density Functional, and Correlated ab Initio Study. *Inorg. Chem.* **2005**, *44*, 5345-5360.

55. Dilworth, J.; Zheng, Y.; Lu, S.; Wu, Q. Preparation and characterization of a novel asymmetrically oxidized complex of 2-(diphenylphosphino)-benzenethiol with ruthenium. The crystal and molecular structure of [Ru(2-Ph$_2$PC$_6$H$_4$S)·(2-Ph$_2$PC$_6$H$_4$S−OH)(2-Ph$_2$PC$_6$H$_4$SO$_2$)]·1/2H$_2$O. *Transition Met. Chem.* **1992**, *17*, 364-368.

56. Grapperhaus, C. A., Kozlowski, M. P., Kumar, D., Frye, N. H., Venna, B. K., Poturovic, S. Singlet Diradical Character of an Oxidized Ruthenium Trithiolate: Electronic Structure and Reactivity. *Angew. Chem. Int. Ed.* **2007**, *46*, 4085-4088.

CURRICULUM VITAE

NAME:	Kagna Ouch
ADDRESS:	University Of Louisville 2320 South Brook Street Louisville, KY, 40292
E. Mail ADDRESS:	kagnaouch@yahoo.com
DOB:	Phnom Penh, Cambodia, September 19, 1983
EDUCATION & TRAINING:	B.S., General Chemistry Royal University of Phnom Penh 2000-2004 M.S., Chemistry University Of Louisville, Louisville, Ky Louisville
PUBLICATIONS:	**Redox-Regulated Ethylene Binding to a Rhenium-Thiolate Complex.** Craig A. Grapperhaus; Kagna Ouch; and Mark S. Mashuta, M. S. manuscript in Preparation